DOI:
10.1016/j.mechmachtheory.2018.09.008

Document Version
Peer reviewed version

Citation for published version (APA):
Lopez-Custodio, P. C., Müller, A., Rico, J. M., & Dai, J. (2018). A synthesis method for 1-DOF mechanisms with a cusp in the configuration space. *Mechanism and Machine Theory*, *132*, 154-175. https://doi.org/10.1016/j.mechmachtheory.2018.09.008

Mechanisms and Machine Theory .
.

A synthesis method for 1-DOF mechanisms with a cusp in the configuration space

P.C. López-Custodio · A. Müller · J.M. Rico · J.S. Dai

Received: date / Accepted: date

Abstract Significant progress has been made in the study of singularities of mechanisms. This research has, however, exclusively focused on situations where different motion branches intersect, i.e. bifurcation points of the configuration space (c-space). Other types of singularities have not been studied due to lack of mechanisms examples. In particular, mechanisms exhibiting cusp singularities in their c-space are almost unknown, besides a planar linkage presented by Connelly and Servatius, which served as an example where the common definition of rigidity fails. In this paper, a method for the synthesis of spatial 1-degree-of-freedom (1-DOF) cusp mechanisms is presented. This method consists in synthesizing the mechanical generator of a spatial curve with specific characteristics and then appropriately connecting this module with its mirrored version. Several examples are presented including a kine-

P.C. López-Custodio
Advanced Kinematics and Reconfigurable Robotics Lab
King's College London
London, UK
E-mail: pablo.lopez-custodio@kcl.ac.uk

A. Müller
Robotics Institute
Johannes Kepler University
Linz, Austria.
E-mail: a.mueller@jku.at

J.M. Rico
División de Ingenierías Campus Irapuato Salamanca
Universidad de Guanajuato
Salamanca, México.
E-mail: jrico@ugto.mx

J.S. Dai
Advanced Kinematics and Reconfigurable Robotics Lab
King's College London
London, UK.
E-mail: jian.dai@kcl.ac.uk

matotropic linkage, which is characterized by a singularity that is a cusp (1 DOF motion) and a bifurcation of a curve and a surface (2-DOF motion). It is discussed that all available methods for the local analysis of singularities fail at cusp singularities. The presented synthesis method allows for constructing mechanisms that shall initiate the research into the study of cusp singularities.

Keywords Kinematics · Configuration space · Cusp · Singularity · Reconfigurability

1 Introduction

Singularities of mechanisms have been widely studied since it was noted that the kinematic properties of a mechanism change suddenly in certain configurations [18, 25, 40, 41]. In the abundance of research made on the topic, several types of singularities have been identified. Of particular significance are configuration space (c-space) singularities where the differential degrees of freedom (DOF) of a mechanism change, called *increased mobility configurations* by Hunt [18]. At such singularities the c-space ceases to be a smooth manifold. Best known are bifurcation singularities or constraint singularities, i.e. intersection points of different branches which allow for reconfiguration [1, 10] of a mechanism. This type of singularities has been widely studied [14, 15, 32, 46]. However, there is a situation that has not at all been studied thoroughly: the presence of cusp singularities in the c-space. The analysis of such singularities is challenging since at a cusp the tangential aspect does not reveal the local c-space geometry, i.e. possible motions, as it does for bifurcations. In particular the tangent space and the tangent cone fail to reveal the first-order and local properties, which is a topic of active research in differential geometry that motivated various definitions of tangent cone.

From a kinematic point of view, at a cusp singularity the mechanism is in a dead point, which means that the velocities of all joints are zero (if it is not a bifurcation point at the same time, in which case only some of the joint velocities must be zero) and the only possibility of motion is a reversal. Since at a cusp singularity, the velocities of all joints are zero, and the mechanism is seemingly rigid, the phenomenon attracted the attention in the field of mathematical rigidity theory. In [8] Connelly and Servatius designed a planar mechanism exhibiting a cusp singularity in its c-space in order to bring a case of a movable linkage which is third-order rigid but not rigid, thus it is a counterexample of the traditional definition of *higher-order rigidity*. This will be called the 'double-Watt mechanism' as it is constructed by combining two Watt linkages. To the best knowledge of the authors, although a few other papers in the field of rigidity addressed the topic [17, 23, 38, 42, 43], no other example of cusp mechanism was presented. In addition, from the point of view of kinematics, the problem of cusp singularities was only discussed in [34].

The lack of examples of similar mechanisms whose c-space has a cusp singularity hinders establishing fundamental research into this phenomenon and finding a way to properly analyze such singularities. Therefore, in this paper

a method for the design of spatial 1-DOF mechanisms with cusp singularities is presented as a means to generate test cases facilitating such research. This method is based in the intersection of surfaces [26–29]. In addition, a planar mechanism with a higher-order cusp singularity is presented using the same idea applied by Connelly and Servatius [8] in the design of the double-Watt mechanism. It will be proved that some of the cusp mechanisms presented in this paper have a complicated c-space in which several regular branches intersect at the cusp singularity, in one of the examples one of these branches is a 2-dimensional manifold which proves that the example is a kinematotropic cusp mechanism. With the exception of the mechanism recently presented by the authors of this paper in [30], this is the first time that spatial mechanisms featuring cusp singularities are presented and also the first time that reconfiguration is carried out through a cusp singularity.

This paper is organized as follows: Firstly, the notation used in this paper is introduced in section 2; in section 3 the cusp mechanism presented by Connelly and Servatius is revisited and a new planar cusp mechanism is presented; the method used in planar curves in section 3 is extended to spatial curves in section 4; the generation of these spatial curves with mechanisms in presented in section 5; in section 6 some examples are presented and analyzed; finally, conclusions are presented in section 7.

2 Notation

The notation used through the paper is now introduced. Three-dimensional vectors are written in lowercase bold letter, such as $\mathbf{v} \in \mathbb{R}^3$. $\mathbf{S} \in \mathbb{R}^6 \cong \mathrm{se}(3)$ is used for screw coordinate vectors, while any other bold capital letter indicates a matrix, such as $\mathbf{R}$. The notation from [9] is used to manage coordinate systems: coordinate systems are named with italic capital letters (e.g. A, B, C...), ${}^{A}\mathbf{r}$, is the vector $\mathbf{r}$ resolve in coordinate system A, ${}^{A}_{B}\mathbf{R} \in SO\,(3)$ is the rotation matrix that relates coordinate system B to coordinate system A, such that ${}^{A}\mathbf{r} = {}^{A}_{B}\mathbf{R}\,{}^{B}\mathbf{r}$. $\{\hat{\mathbf{i}}, \hat{\mathbf{j}}, \hat{\mathbf{k}}\}$ denotes the triad defining a coordinate frame. The derivative with respect to the arc length parameter s is written as $\mathbf{r}'(s) := \mathrm{d}\mathbf{r}/\mathrm{d}s$. In a similar way to coordinate systems, points are presented in italic capital letters, however, point names start at P in the alphabet, with the exception of points E_1 and E_2. $\mathscr{C}$ denotes a curve, while $\mathcal{S}$ denotes a surface. $\{\hat{\mathbf{t}}, \hat{\mathbf{n}}, \hat{\mathbf{b}}\}$ is the Frenet frame of a space curve, while capital $\hat{\mathbf{N}}$ is the normal vector to a surface. We use $\sigma : U \to \mathcal{S}$ for surface parametrization, with $U \subseteq \mathbb{R}^2$. $d(P, Q) \in \mathbb{R}$ is the Euclidean distance between points P and Q, $\mathrm{Rot}(\beta, \hat{\mathbf{v}}) \in \mathrm{SO}(3)$ is the rotation matrix representing a rotation of β radians about an axis that passes through the origin and that is parallel to $\hat{\mathbf{v}}$, $\mathrm{Ref}(\hat{\mathbf{v}}) \in \mathrm{O}(3)$ is the reflection matrix representing a reflection through a plane, with normal vector $\hat{\mathbf{v}}$, containing the origin, i.e. an orthogonal matrix with determinant -1. im() stands for the image of a function. κ and τ are used for curvature and torsion of a curve, respectively, while κ^{n} is used for normal curvature of a surface. α_{i-j} is the angle between axes i and j measured from i to j and a_{i-j} is the (shortest)

distance between axes i and j. $T_P\mathcal{M}$ is the tangent space to $\mathcal{M}$ at P. V is the configuration space of the mechanism and $C^K_{\mathbf{q}}V$ denotes the kinematic tangent cone to V at $\mathbf{q}$.

3 Planar Mechanisms with Cusp Singularities in the C-Space

3.1 The Double-Watt Mechanism

In [8] Connelly and Servatius presented the mechanism shown in figure 1 while trying to address the different problems that stem from the concept of *rigidity*. The mechanism is, to the authors' knowledge, the first example which has a configuration space that features a cusp. This linkage is obtained by merging two 4-bar Watt mechanisms, one being a reflection of the other and then joining the centers of both coupler bars (points P_1 and P_2 in figure 1) with another link.

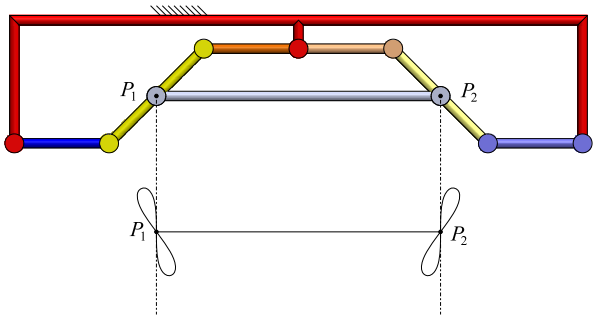

Fig. 1 Double-Watt mechanism presented by Connelly and its generated coupler curves.

The 4-bar Watt mechanism is a line generator [20] as the middle point of the coupler bar draws an 8-shaped curve that approximates a line up to third order at the self-crossing. The curves generated by the couplers of both Watt mechanisms are drawn in figure 1. It can be seen that the mechanism is built so that the reflection line of the mechanism is parallel to the tangents of these curves at the self-crossing. In the shown configuration P_1 and P_2 coincide with the self-crossing of the coupler curves. Despite the presence of the self-crossing, P_1 and P_2 are only able to move through the branch whose tangent is shown and is parallel to the reflection line. Figure 2 shows these branches from both curves connected by the bar $\overline{P_1P_2}$ of length l. The curves have an inflection point at the self-crossings P_1 and P_2, therefore, the horizontal distance between both curves is longer than l above $\overline{P_1P_2}$, equal to l at $\overline{P_1P_2}$, and shorter than l below $\overline{P_1P_2}$. This implies that a circle of radius l centered at Q_1 on the left-hand curve never intersects the other curve if Q_1 is above P_1. It intersects the other curve in one point if $Q_1 = P_1$. If Q_1 is below P_1 the circle intersects the other curve at two points, Q_2 and Q_2'. Therefore, in the last situation, there are

two solutions corresponding to two assembly configurations of the mechanism. Now, as Q_1 gets closer to P_1, Q_2' gets closer to Q_2 until Q_1 reaches P_1 where the two intersections become one and $Q_2' = Q_2 = P_2$ and Q_1 cannot continue moving upwards. This indicates that the mechanism is in a dead point position where all the velocities must be zero since the only possibility of motion is Q_1 moving down again, implying a change in the sign of all joint angles. It can be concluded that the position $Q_1 = P_1$ is a cusp in the configuration space of the double-Watt mechanism. The local higher order analysis of the mechanism at such singularity was presented in [34]. It is important to mention that the length of the coupler bar l is not restricted since the curvature of the drawn curves is zero at the self-crossings, which means that the radius of curvature is infinite. However, the shorter the length l, the better the phenomenon can be appreciated.

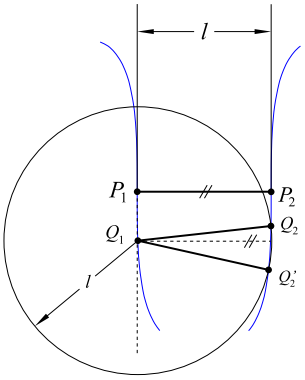

Fig. 2 Curves generated by the coupler bars of both 4-bar Watt loops in the Connelly mechanism.

3.2 Generalization to Other Planar Mechanisms

Any planar mechanism that draws a curve with an inflection point can be used to obtain a cusp mechanism following the same idea. Figure 3 shows an example of Evans mechanism [12] which is a planar 4-bar mechanism whose coupler point P_1 approximates a straight line. In this example of Evans mechanism the coupler curve presents an inflection point where the curve intersects the axis of the revolute joint that connects the fixed link with the input link of length 1. The tangent to the coupler curve at such point is the horizontal line shown in figure 3.

Since the coupler curve has an inflection point, this Evans mechanism can be used to obtain a planar cusp mechanism like the one shown in figure 4, where the 4-bar mechanism has been mirrored through a line parallel to the tangent to the coupler curve at the inflection point. At the cusp singularity,

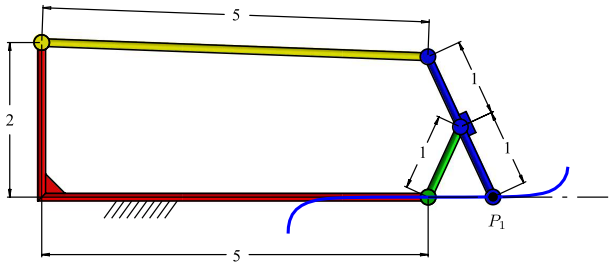

Fig. 3 An example of Evans straight line mechanism.

$\mathbf{q}_0$, the coupler points P_1 and P_2 coincide with the inflection points of the coupler curves as shown in figure 4a).

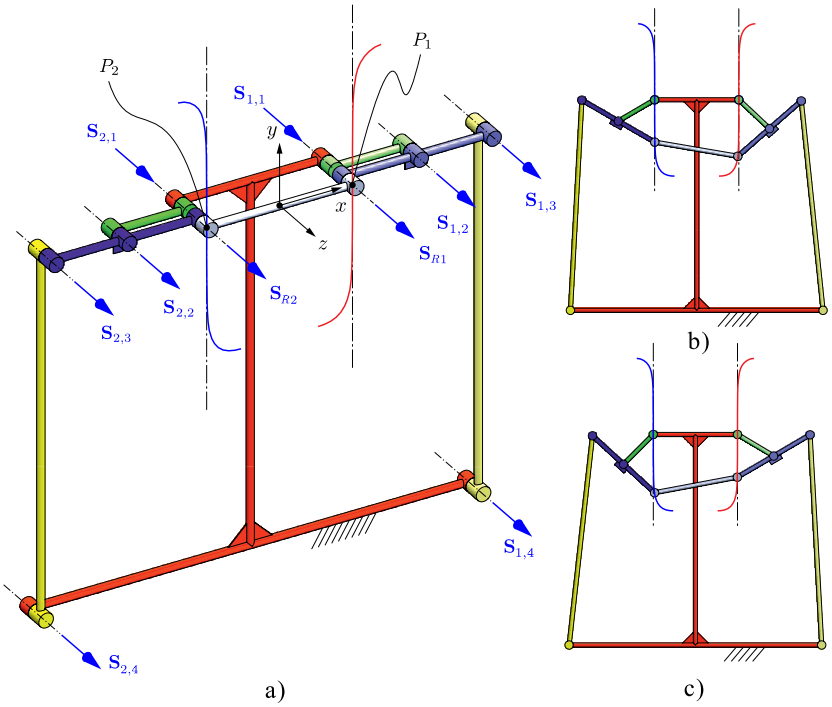

Fig. 4 The double-Evans cusp mechanism: a) Cusp singularity. b) and c) two configurations near the cusp.

Cusp singularities of algebraic curves correspond to multiple solutions of the defining algebraic equations. In the above construction, the c-space is defined by the constitutive constraint equations of the two individual linkages and by the additional constraint due to the connecting link. With this construction it is clear that the order of tangency at the cusp (and thus the multiplicity of the solution) depends on the order up to which the coupler

curves resemble a straight line. In the example in section 3.1, the double-Watt mechanism, the coupler curves are second-order approximations of straight lines at the inflection point. Consequently, at the cusp, when moving toward and when returning from the cusp, the velocity and acceleration of the Double-Watt linkage must vanish. This observation has led Connelly and Servatius [8] to question the notion of higher-order rigidity as it is established in rigidity theory since the Double-Watt is finitely mobile although it does not allow for second- and third-order motions. The order of tangency of the two coupler curves determine the order of the cusp.

The coupler curve of the Evans mechanism shown in figure 3 approximates a straight line up to the fifth-order. This can be proved by obtaining the higher-order derivatives of the position vector of point P_1 and noting that the first four derivatives are parallel to the approximated straight line and the fifth-order derivative is the first one that is non-parallel. Hence, it is expected that the c-space of the double-Evans mechanism shown in figure 4 features a fifth-order cusp. This can be established by a higher-order approximation of possible finite motions through this configuration, i.e. by computing the tangents to the corresponding curves in c-space. The mathematical framework is the kinematic tangent cone $C^{\mathrm{K}}_{\mathbf{q}_0}V$ that can be determined in terms of the instantaneous joint screw coordinates [33, 34]. The instantaneous joint screws in the configuration $\mathbf{q}_0$ are

$$\begin{array}{ll}
\mathbf{S}_{1,1}(\mathbf{q}_0) = (0,0,1;0,-1,0), & \mathbf{S}_{2,1}(\mathbf{q}_0) = (0,0,1;0,1,0) \\
\mathbf{S}_{1,2}(\mathbf{q}_0) = (0,0,1;0,-2,0), & \mathbf{S}_{2,2}(\mathbf{q}_0) = (0,0,1;0,2,0) \\
\mathbf{S}_{1,3}(\mathbf{q}_0) = (0,0,1;0,-3,0), & \mathbf{S}_{2,3}(\mathbf{q}_0) = (0,0,1;0,3,0) \\
\mathbf{S}_{1,4}(\mathbf{q}_0) = (0,0,1;-5,-3,0), & \mathbf{S}_{2,4}(\mathbf{q}_0) = (0,0,1;-5,3,0) \\
\mathbf{S}_{R1}(\mathbf{q}_0) = (0,0,1;0,-1,0), & \mathbf{S}_{R2}(\mathbf{q}_0) = (0,0,1;0,1,0).
\end{array}$$

It is found that there are non-trivial differential motions up to fifth order, whereas $C^{\mathrm{K}}_{\mathbf{q}_0}V = \{\mathbf{0}\}$. Nevertheless, it can be shown that the linkage is finitely mobile with 1 DOF as demonstrated in [35] for Connelly's mechanism.

4 Generation of Spatial Curves Whose Projections on Certain Planes Exhibit Inflection Points

4.1 The Basic Principle

The phenomenon occurring in the 8-shaped curves generated by the double-Watt mechanism can be obtained for curves in E^3. Consider a curve $\mathscr{C}_1$, which can be projected onto a plane Π in such a way that the resulting projection has an inflection point (figure 5). Trace the tangent to the projected curve at the inflection point, then take a vector $\hat{\mathbf{n}}$ perpendicular to this tangent and fix a plane ρ with normal $\hat{\mathbf{N}}_\rho = \hat{\mathbf{n}}$ and located a distance $l/2$ from the inflection point. Now reflect $\mathscr{C}_1$ through ρ to obtain a curve $\mathscr{C}_2$. It can be seen that the projection of both curves onto Π is similar to the array of curves in figure 2.

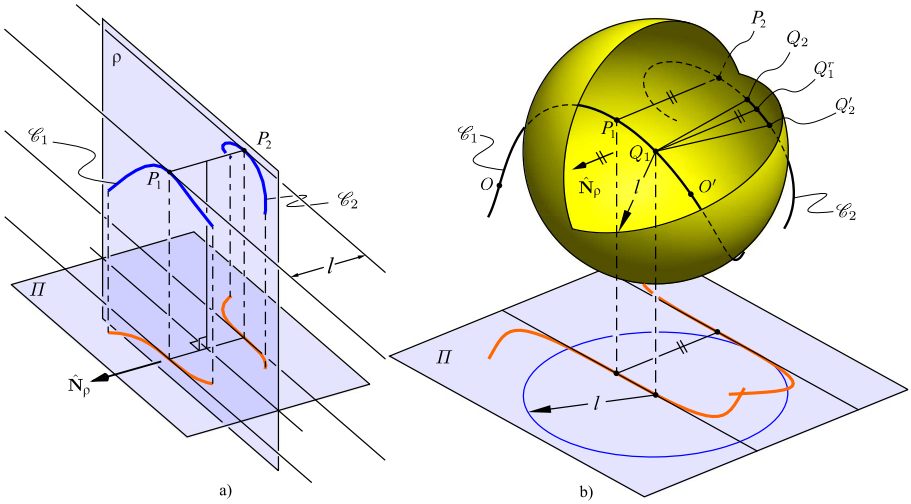

Fig. 5 a) A curve (and its reflection) in 3-space which can be projected onto a plane as a curve with an inflection point. b) A sphere of radius l and center moving through such curve.

P_1 and P_2 are the points whose projections onto Π are the inflection points, thus the distance between them is l.

Now, the case of a sphere of radius l whose center Q_1 is moving through $\mathscr{C}_1$ is analyzed. Refer to figure 5b), the points O and O' lie on the curve $\mathscr{C}_1$, such that P_1 lies on the segment of $\mathscr{C}_1$ between O and O'. If Q_1 is located between points O and P_1 in figure 5b), then the projection of the sphere onto Π is a circle of radius l and center lying on the projection of $\mathscr{C}_1$. Such circle does not intersect the projection of $\mathscr{C}_2$, as explained in the section 3.1. Therefore, the sphere does not intersect $\mathscr{C}_2$ as their projections do not intersect, the converse is not necessary true. For the case when Q_1 is located between points P_1 and O' in figure 5b), consider the line segment $\overline{Q_1Q_1^r}$, where Q_1^r is the reflection of Q_1 through ρ. Then $\overline{Q_1Q_1^r}$ is parallel to $\hat{\mathbf{N}}_\rho$ and, hence, its projection onto Π has the same length. On Π it is clear that such projected segment is shorter than l, and therefore $d(Q_1, Q_1^r) < l$. Thus Q_1^r is inside the sphere with center Q_1 and radius l and $\mathscr{C}_2$ must intersect this sphere at two points Q_2 and Q_2'. As Q_1 gets closer to P_1, Q_2 and Q_2' get closer to each other until $Q_1 = P_1$ when both points coincide, i.e. $Q_2 = Q_2' = P_2$. This indicates that the solution has a cusp.

A well-known fact [22] is that, given a curve in Euclidean 3-space, its projection onto the rectifying plane at a certain point can feature an inflection point. However, this does not apply to every point on the curve, this is proved in Lemma 1[1].

[1] In the literature, this proof is usually made considering only the first four terms of the Taylor expansion and approximating the projected curve to a cubic curve.

Lemma 1. *The projection of a curve onto the rectifying plane at a point P has an inflection point if and only if, it has non-zero torsion at P.*

Proof Let $\alpha(s) \in \mathbb{R}^3$ be the arc-length parametrization of a curve $\mathscr{C} := \text{im}(\alpha([a,b])),\ [a,b] \subseteq \mathbb{R}$, then, for any point $s = s_o$ where $\alpha(s)$ is C^2, the following holds:

$$\begin{aligned}
\alpha'(s_o) &= \hat{\mathbf{t}}(s_o),\\
\alpha''(s_o) &= \kappa(s_o)\hat{\mathbf{n}}(s_o),\\
\alpha'''(s_o) &= -\kappa(s_o)^2\hat{\mathbf{t}}(s_o) + \kappa(s_o)\hat{\mathbf{n}}(s_o) + \kappa(s_o)\tau(s_o)\hat{\mathbf{b}}(s_o),
\end{aligned} \tag{1}$$

where $\hat{\mathbf{t}}(s_o)$, $\hat{\mathbf{n}}(s_o)$ and $\hat{\mathbf{b}}(s_o)$ are the tangent, normal and binormal vectors of the Frenet frame at $s = s_o$ and κ and τ, the corresponding curvature and torsion at such point, respectively. Choose[2] $s_o = 0$, using the arc-length derivatives from Eq. (1) the Taylor expansion of $\alpha(s)$ around $s_o = 0$ is given by

$$\begin{aligned}
\alpha(s) &= s\alpha'(0) + \frac{s^2}{2}\alpha''(0) + \frac{s^3}{6}\alpha'''(0) + \sum_{i=4}^{\infty}\frac{s^i}{i!}\alpha^{(i)}(0),\\
&= \left[s - \frac{1}{6}\kappa(0)^2 s^3 + \sum_{i=4}^{\infty}\frac{s^i}{i!}\alpha^{(i)}(0)\cdot\hat{\mathbf{t}}(0)\right]\hat{\mathbf{t}}(0) +\\
&\quad + \left[\frac{1}{2}\kappa(0)s^2 + \frac{1}{6}\kappa(0)s^3 + \sum_{i=4}^{\infty}\frac{s^i}{i!}\alpha^{(i)}(0)\cdot\hat{\mathbf{n}}(0)\right]\hat{\mathbf{n}}(0) +\\
&\quad + \left[\frac{1}{6}\kappa(0)\tau(0)s^3 + \sum_{i=4}^{\infty}\frac{s^i}{i!}\alpha^{(i)}(0)\cdot\hat{\mathbf{b}}(0)\right]\hat{\mathbf{b}}(0)
\end{aligned} \tag{2}$$

Let $\gamma(s) \in \mathbb{R}^2$ be a parametrization of the projection of $\mathscr{C}$ onto the rectifying plane at $s = 0$, which is spanned by the tangent and binormal vectors, then

$$\begin{aligned}
\gamma(s) = \Bigg(&s - \frac{1}{6}\kappa(0)^2 s^3 + \sum_{i=4}^{\infty}\frac{s^i}{i!}\alpha^{(i)}(0)\cdot\hat{\mathbf{t}}(0),\\
&\frac{1}{6}\kappa(0)\tau(0)s^3 + \sum_{i=4}^{\infty}\frac{s^i}{i!}\alpha^{(i)}(0)\cdot\hat{\mathbf{b}}(0)\Bigg)
\end{aligned} \tag{3}$$

where the $x-$ and $y-$coordinates are taken along $\hat{\mathbf{t}}(0)$ and $\hat{\mathbf{b}}(0)$, respectively.

To prove that $s = 0$ is a potential inflection point, we consider the curvature of $\gamma(s)$, which has to be zero at an inflection point. Zero curvature in a planar parametric curve implies that $f(s) := x'(s)y''(s) - y'(s)x''(s)$ vanishes at $s = 0$. From Eq (3), it follows that $\gamma'(0) = (1,0)$ and $\gamma''(0) = (0,0)$, therefore $f(0) = 0$. However, at an inflection point the curvature is not only zero, but it

[2] The proof can be made for $s_o = 0$ without loss of generality since we can always define another arc-length parametrization $\beta : [a,b] \to \mathbb{R}^3$, such that $\beta(s) = \alpha(s + s_o)$, then $\beta(0) = \alpha(s_o)$

is also changing its sign, thus $f'(s) \neq 0$ at $s = 0$ is required. After derivation it follows that $f'(0) = -\kappa(0)\tau(0)$. Notice that $\kappa(0)$ is the curvature of $\mathscr{C}$ at $s = 0$. In order to define the Frenet apparatus it is required that $\kappa(0) \neq 0$, however $\tau(0) = 0$ is possible and would imply that the projected curve does not present an inflection point at $s = 0$. It is concluded that the projection of a curve onto the rectifying plane at a point has an inflection point if and only if it has non-zero torsion at such point. ■

4.2 Generating Curves with Inflection Points by Projecting the Intersection of Surfaces

The manipulation of curves becomes easy when considering them as the intersection of two surfaces. The Frenet apparatus can be computed using the local properties of the surfaces [45]. Hence, it is not required to find a parametrization of the intersection curve as long as the parameterizations or implicit forms of the surfaces are known and local properties, i.e. normal vector, principal directions and principal normal curvatures, are available.

Figure 6a) shows a curve $\mathscr{C}_1$ obtained by intersecting two cylinders, $\mathcal{S}_1^A$ and $\mathcal{S}_1^B$. At the point P_1 with non-vanishing torsion, the Frenet frame is shown. The curve is projected onto a plane $\mathit{\Pi}$ parallel to the rectifying plane at P_1. The resulting 8-shaped planar curve has an inflection point at the projection of P_1. Thus, following the idea previously explained, $\mathcal{S}_2^A$ and $\mathcal{S}_2^B$ are the reflections of $\mathcal{S}_1^A$ and $\mathcal{S}_1^B$, respectively, and their intersection, $\mathscr{C}_2$ is a reflection of $\mathscr{C}_1$. On the other hand, figure 6b) shows the same curve and its Frenet frame at a zero-torsion point, Q. The projection of $\mathscr{C}_1$ onto the rectifying plane leads to a curve with zero curvature at the projection of Q, however, this is not an inflection point.

An even simpler way of obtaining a projection with an inflection point is using spatial 8-shaped curves or 2-winged curves with two planes of symmetry. These can be easily obtained by intersecting surfaces that become tangent to each other at an isolated point, this point becomes the self-crossing of the 8-shaped curve. Figure 7 shows the Viviani curve, $\mathscr{C}$, obtained from the intersection of a cylinder, $\mathcal{S}^A$, and a sphere , $\mathcal{S}^B$, which are tangent to each other at P, and, hence, they have the same normal vector $\hat{\mathbf{N}}$ at such point. $\mathscr{C}$ has two planes of symmetry which contain $\hat{\mathbf{N}}$. Let $\mathit{\Pi}$ be a plane parallel to $T_P\mathcal{S}^A = T_P\mathcal{S}^B$, and, therefore, having normal $\hat{\mathbf{N}}$, then the projection of $\mathscr{C}$ onto $\mathit{\Pi}$ is a symmetric 8-shaped planar curve with two branches intersecting at the projection of P onto $\mathit{\Pi}$. Each branch has an inflection point and considering the two tangent vectors $\hat{\mathbf{t}}_1$ and $\hat{\mathbf{t}}_2$ there are two possible planes that can be used to reflect both surfaces.

It is not necessary to calculate a parametrization of $\mathscr{C}$ since $\hat{\mathbf{t}}_1$ and $\hat{\mathbf{t}}_2$ can be obtained from the local properties of $\mathcal{S}_A$ and $\mathcal{S}_B$, namely, the principal curvatures and common normal vector. The normal curvature of both surfaces is the same at P in the $\hat{\mathbf{t}}_1$ and $\hat{\mathbf{t}}_2$ directions, hence, using Euler's formula [21] for normal curvature it follows:

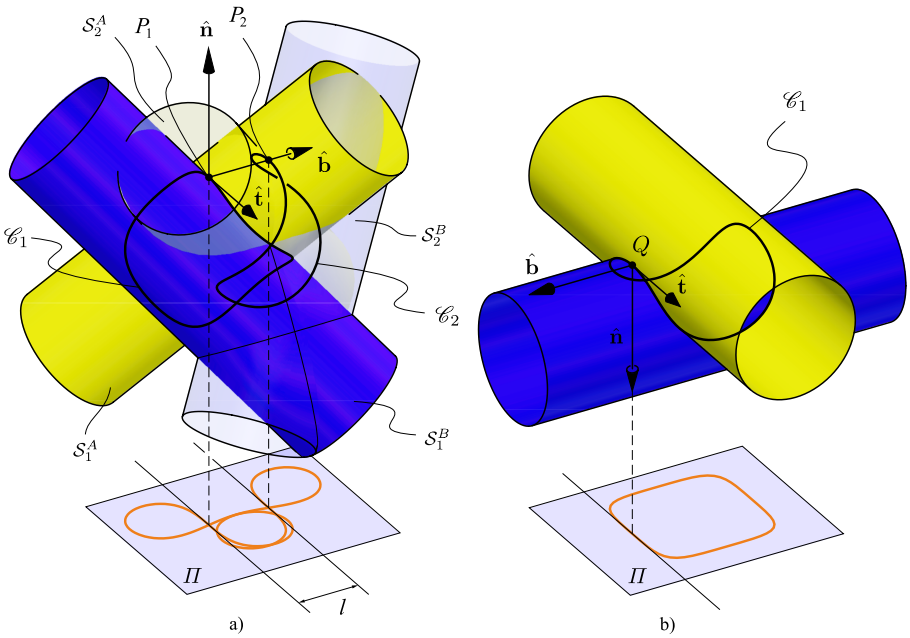

Fig. 6 The curve $\mathscr{C}_1$ as the intersection of two cylinders and its projection onto rectifying plane. a) The projection happens at a non-zero torsion point and the surfaces are reflected. b) The projection occurs at a zero-torsion point.

$$\kappa^{\mathrm{n}}_{A,1}\cos^2\phi_A + \kappa^{\mathrm{n}}_{A,2}\sin^2\phi_A = \kappa^{\mathrm{n}}_{B,1}\cos^2\phi_B + \kappa^{\mathrm{n}}_{B,2}\sin^2\phi_B \tag{4}$$

where, for $i = A, B$, $\kappa^{\mathrm{n}}_{i,1}$ and $\kappa^{\mathrm{n}}_{i,2}$ are the principal normal curvatures of $\mathcal{S}^i$, and ϕ_i is the angle from the principal direction $\hat{\mathbf{e}}_{i,1}$ to some tangent to the intersection curve. Since all principal directions, $\hat{\mathbf{e}}_{A,1}$, $\hat{\mathbf{e}}_{A,2}$, $\hat{\mathbf{e}}_{B,1}$ and $\hat{\mathbf{e}}_{B,2}$ are expected to be known, a linear restriction $\phi_B(\phi_A)$ is known and can be substituted in Eq. (4) to obtain one non-linear equation in the unknown ϕ_A. For this case, two solutions are expected, each related to the respective tangent to the intersection curve. If (4) has no solution, the surfaces are touching at P, which is in such case an isolated point (intersection in one point). If (4) has a double root, then the intersection of the surfaces is a curve containing P.

5 Construction of cusp mechanisms

5.1 Mechanical Generators for the Intersection of Surfaces

It is known [7, 31, 39] that symmetric spatial 8-shaped curves, similar to the Viviani curve, can be traced by coupler points of spherical 4-bar and crank-slider mechanisms. However, from the previous discussion it is clear that the use of intersection curves can ease the design of mechanisms with cusps in the

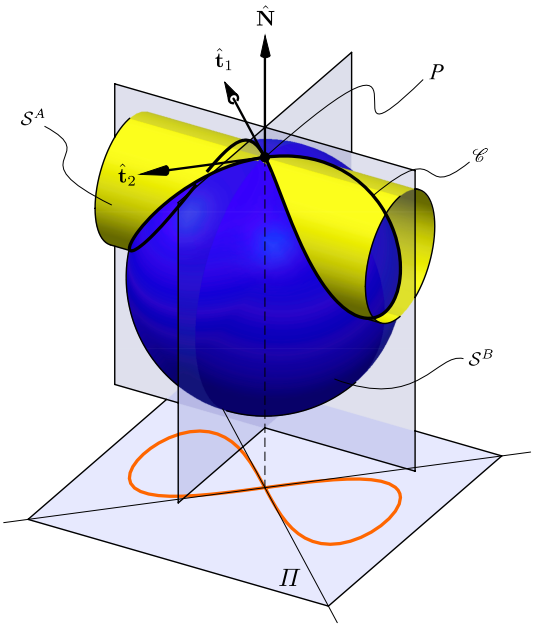

Fig. 7 The Viviani curve as an intersection of surfaces and its projection onto a plane parallel to the tangent plane at the self-crossing.

configuration space. The first step is to generate the appropriate surfaces by using two kinematic dyads, and the second step is to appropriately connect them so to form a 1-DOF closed loop mechanism.

A variety of surfaces can be generated by the end link of kinematic dyads. These surfaces can be ruled surfaces (one of the kinematic pairs is a prismatic joint), surfaces of revolution (the first joint is a revolute) or helical surfaces (the first kinematic pair is a helical joint), among other forms. If P,R and H stand for prismatic, revolute and helical joints, respectively, planes (PP), hyperboloids (RP), toroids (RR), helicoids (HP), etc. can be generated by the end effector of kinematic dyads, see [44] for an exhaustive table of the surfaces that can be generated by kinematic dyads.

Let A and B be two kinematic dyads, whose points E_1^A and E_1^B, defined at the end links, generate the surfaces $\mathcal{S}_1^A$ and $\mathcal{S}_1^B$, respectively. If the end links of both dyads are connected so that $E_1 := E_1^A = E_1^B$, then E_1 is confined to move on $\mathcal{S}_1^A \cap \mathcal{S}_1^B$. The end link must be connected by an adequate number of revolute joints with axes meeting E_1 to allow for the necessary relative rotation between the end links. Since the position of E_1^A and E_1^B is enforced to coincide with E_1, no further kinematic joints are required to ensure the 1-DOF motion of the closed loop mechanism.

Figure 8 shows the four possible cases depending on the number of revolute joints intersecting E_1 that are required to make the linkage mobile. If the number of these revolute joints is three, the resulting mechanism has seven kine-

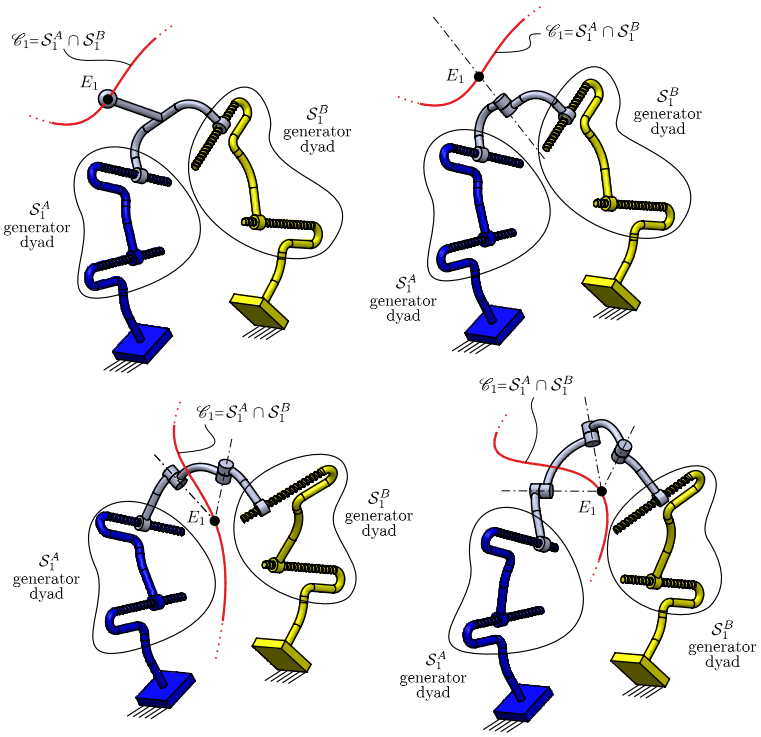

Fig. 8 The four different cases of one-loop mechanisms obtained from the intersection of surfaces.

matic pairs and it is non-overconstrained. However, if less than three revolute joints are required to join E_1 and E_2, then the mechanism is overconstrained. The number of these revolute joints is always 2 or 1 for the intersection of ruled surfaces as well as in cases when one of the surfaces is a plane. In some other cases where certain constraints between the construction parameters of the surfaces lead to special symmetries, the number of revolute joints intersecting at E_1 (respectively E_2) can be reduced to 2 or 1, and the mechanism becomes a paradoxical mechanism [2, 16, 36]. An example is shown in Section 6 where the intersection of two toroids leads to a Bricard plane-symmetric paradoxical 6R mechanism.

5.2 Interconnection of the Curve Generator with its Mirrored Copy

Once a mechanism is defined whose coupler curve $\mathscr{C}_1 \subseteq \mathcal{S}_1^A \cap \mathcal{S}_1^B$ can be projected onto a plane such that at certain point P_1 the projected curve has an inflection, this mechanism is mirrored so that the new generated surfaces, $\mathcal{S}_2^A$ and $\mathcal{S}_2^B$, are reflections of $\mathcal{S}_1^A$ and $\mathcal{S}_1^B$, as explained in Section 4. The reflected closed-loop kinematic chain consist of two dyads joined by an adequate number of revolute joints with axes meeting at point E_2 that generates the intersection

curve $\mathscr{C}_2$. Finally, points E_1 and E_2 are joined with a coupler bar of length l. The length l is not restricted as explained in section 3.1. This bar is connected to the two curve generator mechanisms by means of a spherical pair (S) at one of its ends and a universal joint (U) at the other end. These allow unlimited relative rotations of the curve generators, while the U joint eliminates a passive degree of freedom that would be present if both ends of the coupler bar were connected by S joints. Namely, the bar could spin about its longitudinal axis. It is also possible to connect the two curve generator mechanisms by means of a URU kinematic chain where the axis of the R joint intersects the centers of the U joints.

With the above described construction, the generated mechanism possesses three topologically independent loops as shown in figure 9.

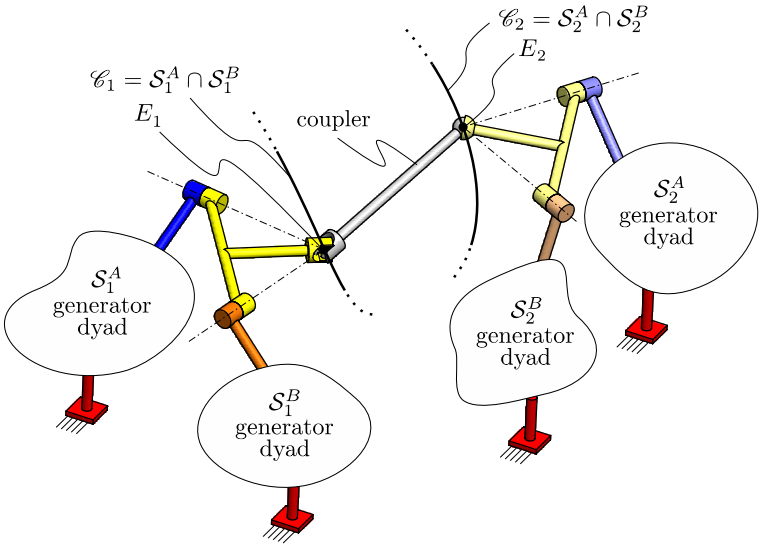

Fig. 9 The general form of a cusp mechanism in the case in which two revolute joints allow the motion about E_1 and E_2 at $\mathscr{C}_1$ and $\mathscr{C}_2$, respectively.

5.3 Summary of the Proposed Method

The procedure discussed in the previous section can be summarized as a set of steps to obtain spatial mechanisms with a cusp in the configuration space.

1. Find two surfaces, $\mathcal{S}_1^A$ and $\mathcal{S}_1^B$, that can be generated by kinematic dyads and whose intersection curve $\mathscr{C}_1$ can be projected onto a plane Π to obtain an inflection point. Fix $P_1 \in \mathscr{C}_1$ at the point whose projection is the inflection point.
2. Find the tangent vector $\hat{\mathbf{t}}$ to the curve at P_1.

3. Define a reflection plane ρ perpendicular to Π, with normal being perpendicular to $\hat{\mathbf{t}}$ and placed a distance $l/2$ from P_1.
4. Design a 1-loop mechanism that generates $\mathscr{C}_1$: obtain kinematic dyads that generate $\mathcal{S}_1^A$ through E_1^A and $\mathcal{S}_1^B$ through E_1^B, join their end-links so that $E_1 = E_1^A = E_1^B$ with the required number of revolute joints with axes intersecting E_1.
5. Mirror the mechanism through ρ. The point E_2 in the reflected mechanism generates $\mathscr{C}_2$.
6. Join points E_1 and E_2 with a coupler bar of length l with a spherical (S) joint at one of its endings and a universal joint (U) in the other. The result is a 1-DOF 3-loop cusp mechanism. The coupler bar is connected via S and U joints in order to avoid a passive motion of the bar (spinning about its longitudinal axis that would be introduced if two S joints were used). In the case that the generated curves are planar the coupler bar is connected to the two curve generators by means of revolute joints with axes that are perpendicular to the plane that contains the curves.

6 Examples

In this section three examples of spatial cusp mechanisms are presented. Each step from section 5.3 is described. The screws of the joints in the mechanism are presented for the cusp configuration $\mathbf{q}_0 \in V$. For that aim, a coordinate frame 0 is fixed with origin in the middle point of $\overline{P_1P_2}$ and with y_0-axis perpendicular to the reflection plane ρ. At the cusp configuration, the joint screw coordinate vectors of the mechanism generating $\mathscr{C}_1$ are determined in coordinate frame 0, denoted with ${}^0\mathbf{S}_{1,i} := ({}^0\hat{\mathbf{s}}_{1,i};\, {}^0\mathbf{r}_{1,i} \times {}^0\hat{\mathbf{s}}_{1,i} + h_{1,i}{}^0\hat{\mathbf{s}}_{1,i})$, $i = 1, \ldots, 5$. Finding ${}^0\mathbf{S}_{2,i}$, $i = 1, \ldots, 5$ becomes easy since ${}^0\hat{\mathbf{s}}_{2,i} = \mathrm{Ref}(\hat{\mathbf{j}})\,{}^0\hat{\mathbf{s}}_{1,i}$, ${}^0\mathbf{r}_{2,i} = \mathrm{Ref}(\hat{\mathbf{j}})\,{}^0\mathbf{r}_{1,i}$ and $h_{2,i} = -h_{1,i}$. Since screw coordinates are always represented in the coordinate frame 0, the reference to this frame is omitted: ${}^0\mathbf{S} = \mathbf{S}$.

6.1 A Spatial Mechanism Generating Planar Curves

Step 1: Two frames, A_1 and B_1, are defined as shown in figure 10a). $\mathcal{S}_1^A := \mathrm{im}(\sigma_1^A(\mathbb{R}^2))$, where ${}^{A_1}\sigma_1^A(u, v) := (u, v, 0)$, is a plane. $\mathcal{S}_1^B := \mathrm{im}(\sigma_1^B(\mathbb{R}^2))$, where ${}^{B_1}\sigma_1^B(u, v) := (d\cos u, v, hu)$, is the result of extruding a cosine curve in the $x_1^B z_1^B$ plane through the y_1^B axis. This surface looks like a corrugated roof. The origins of frames A_1 and B_1 coincide and ${}^{A_1}_{B_1}\mathbf{R} := \mathrm{Rot}\,(\pi/6, \hat{\imath})$ as shown in figure 10a). $\mathscr{C}_1 = \mathrm{im}(\alpha(\mathbb{R}))$, where ${}^{A_1}\alpha(u) := (d\cos u, 2hu, 0)$ is a cosine function in the $x_1^A y_1^A$ plane. Such planar curve has an inflection point whenever it crosses the y_1^A-axis. We can choose any of these points and fix P_1 there, as shown in figure 10c). In this example we consider $d = 10$ and $h = 5/(2\pi)$.

Step 2: ${}^{A_1}\hat{\mathbf{t}} = (1/k, -2\pi/k, 0)$, where $k = \sqrt{1 + 4/\pi^2}$.

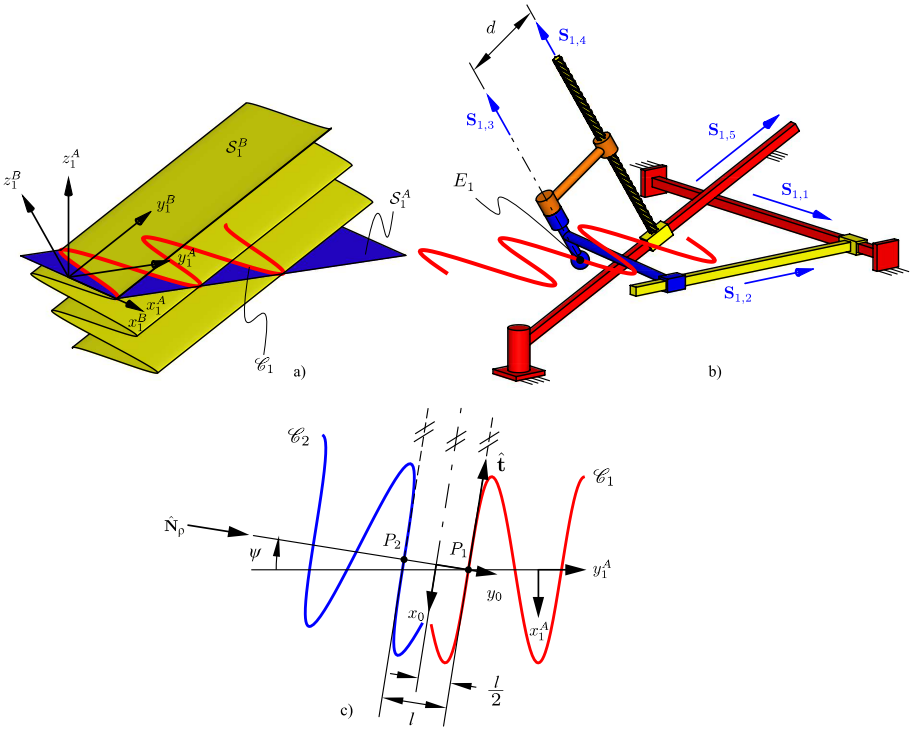

Fig. 10 The intersection of two surfaces that leads to a planar curve with inflection points. a) Surfaces setup. b) Overconstrained mechanism that generates such curve. c) Reflection of the intersection curve

Step 3: $\hat{\mathbf{N}}_\rho$ lies on $x_1^A y_1^A$ and is perpendicular to $\hat{\mathbf{t}}$ as shown in figure 10c). The orientation of coordinate system 0 with respect to A_1 is given by ${}^{A_1}_{0}\mathbf{R} = \mathrm{Rot}(\psi, \hat{\mathbf{k}})$, with $\psi = \arctan(2\pi)$.

Step 4: $\mathcal{S}_1^A$ is generated by a pair of prismatic joints with axes parallel to any non-parallel vectors in $x_1^A y_1^A$ plane. $\mathcal{S}_1^B$ is generated by $\{\mathbf{S}_{1,5}, \mathbf{S}_{1,4}\}$ (see figure 10b), where $\mathbf{S}_{1,5}$ represents a prismatic joint with axis parallel to y_1^B and $\mathbf{S}_{1,4}$ represents a helical joint of pitch h and axis perpendicular to $\mathbf{S}_{1,5}$. $\mathcal{S}_1^B$ is generated by a point E_1 fixed to the end link and located a distance d from $\mathbf{S}_{1,4}$ (see [19]). E_1^A and E_1^B are joined by a single revolute joint with axis $\mathbf{S}_{1,3}$ passing through E_1. This revolute joint compensates the rotation of the helical joint, so that $\mathrm{d}^n q_{1,4}/\mathrm{d}t^n = -\mathrm{d}^n q_{1,3}/\mathrm{d}t^n$, $\forall n \in \mathbb{Z}$.

Steps 5 and 6: Figure 11a) shows the 3-loop mechanism obtained after mirroring the overconstrained linkage, obtained in step 4, through a plane perpendicular to the z-axis and containing the origin O. The two mechanisms are connected through a coupler bar of length $l = 7$. Since $\mathscr{C}_1$ and $\mathscr{C}_2$ are planar curves, the coupler bar is attached via revolute joints with axes $\mathbf{S}_{R1}$ and $\mathbf{S}_{R2}$ parallel to z_1^A. The topological graph is shown in figure 11b).

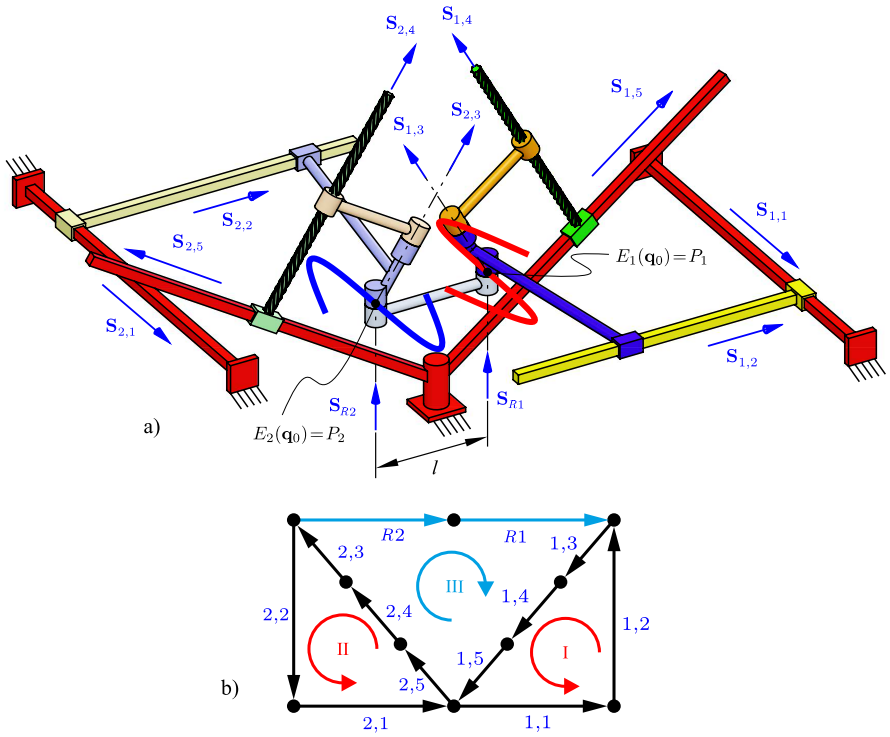

Fig. 11 a) A mechanism that generates two planar curves of the cosine form in a cusp configuration. b) Topological graph

Analysis of smooth motions through $\mathbf{q}_0$: The screw coordinates at the cusp are

$$\mathbf{S}_{1,1}(\mathbf{q}_0) = (0,\ 0,\ 0;\ 1,\ 0,\ 0),$$
$$\mathbf{S}_{1,2}(\mathbf{q}_0) = (0,\ 0,\ 0;\ 0,\ 1,\ 0),$$
$$\mathbf{S}_{1,3}(\mathbf{q}_0) = \left(\frac{1}{2k},\ -\frac{\pi}{k},\ \frac{\sqrt{3}}{2};\ \frac{7\sqrt{3}}{2},\ 0,\ -\frac{7}{4k}\right),$$
$$\mathbf{S}_{1,4}(\mathbf{q}_0) = \left(\frac{1}{2k},\ -\frac{\pi}{k},\ \frac{\sqrt{3}}{2};\ \frac{7\pi\sqrt{3}k+80\pi^2+5}{4\pi k},\ \frac{15}{2k},\ \frac{20\sqrt{3}\pi^2-7\pi k+5\sqrt{3}}{16\pi^3+4\pi}\right),$$
$$\mathbf{S}_{1,5}(\mathbf{q}_0) = \left(0,\ 0,\ 0;\ -\frac{\sqrt{3}}{2k},\ \frac{\sqrt{3}\pi}{k},\ \frac{1}{2}\right),$$
$$\mathbf{S}_{2,1}(\mathbf{q}_0) = (0,\ 0,\ 0;\ 1,\ 0,\ 0),$$
$$\mathbf{S}_{2,2}(\mathbf{q}_0) = (0,\ 0,\ 0;\ 0,\ 1,\ 0),$$
$$\mathbf{S}_{2,3}(\mathbf{q}_0) = \left(\frac{1}{2k},\ \frac{\pi}{k},\ \frac{\sqrt{3}}{2};\ -\frac{7\sqrt{3}}{4},\ 0,\ \frac{7}{4k}\right),$$

$$\mathbf{S}_{2,4}(\mathbf{q}_0) = \left(\frac{1}{2k},\ \frac{\pi}{k},\ \frac{\sqrt{3}}{2};\ \frac{-7\pi\sqrt{3}k - 80\pi^2 - 5}{4\pi k},\ \frac{15}{2k},\ \frac{-20\sqrt{3}\pi^2 + 7\pi k - 5\sqrt{3}}{16\pi^3 + 4\pi}\right),$$

$$\mathbf{S}_{2,5}(\mathbf{q}_0) = \left(0,\ 0,\ 0;\ -\frac{\sqrt{3}}{2k},\ -\frac{\sqrt{3}\pi}{k},\ \frac{1}{2}\right),$$

$$\mathbf{S}_{R1}(\mathbf{q}_0) = \left(0,\ 0,\ 1;\ \frac{7}{2},\ 0,\ 0\right),$$

$$\mathbf{S}_{R2}(\mathbf{q}_0) = \left(0,\ 0,\ 1;\ -\frac{7}{2},\ 0,\ 0\right).$$

The kinematic tangent cone is therewith found to be $C^{\mathrm{K}}_{\mathbf{q}_0} V = \{\mathbf{0}\}$. That is, there is no smooth curve passing through the singular reference configuration.

6.2 A Double-Koenigs Mechanism

Step 1: $\mathcal{S}_1^A := \mathrm{im}(\sigma_1^A(\mathbb{T}\times\mathbb{R}))$, where ${}^{A_1}\sigma_1^A(u,v) := (v, d\cos u, d\sin u)$, is a right cylinder (with axis being perpendicular to the plane that contains the circle) of radius d and with axis along x_1^A and $\mathcal{S}_1^B := \mathrm{im}(\sigma_1^B(\mathbb{T}\times\mathbb{R}))$, where ${}^{B_1}\sigma_1^B(u,v) := (v, (d/2)\cos u, (d/2)\sin u)$, is another right cylinder with radius $d/2$ and axis along x_1^B. The origin of frame B_1 with respect to the origin of frame A_1 is displaced by ${}^{A_1}\mathbf{r}_{B_1/A_1} = (0,0,d/2)$ and their relative orientation is given by ${}^{A_1}_{B_1}\mathbf{R} := \mathrm{Rot}(\pi/2, \hat{\mathbf{k}})$ as shown in figure 12a). $\mathscr{C}_1$ is an 8-shaped curve with two planes of symmetry. Therefore, its projection onto the $x_1^A y_1^A$ plane has an inflection point at the projection of the self-crossing. We set P_1 at the self crossing, as shown in figure 12c). For this example we consider $d = 2$.

Step 2: $\hat{\mathbf{t}}_1$ and $\hat{\mathbf{t}}_2$ are obtained using Eq. (4). Since the cylinders are surfaces of revolution, the principal curvatures are the curvatures of the meridians and parallels passing through the point. Hence, $\kappa^{\mathrm{n}}_{A,1} = d$, $\kappa^{\mathrm{n}}_{A,2} = 0$ and $\kappa^{\mathrm{n}}_{B,1} = d/2$ and $\kappa^{\mathrm{n}}_{B,2} = 0$. Two solutions are found for equations (4): $\phi_{A,1} = \pi/2 - \arccos(\sqrt{6}/3)$ and $\phi_{A,2} = 3\pi/2 - \arccos(\sqrt{6}/3)$. We choose $\psi = \phi_{A,1}$, the angle between $\hat{\mathbf{t}}_1$ and the x_1^A axis, as shown in figure 12c). Then, ${}^{A_1}\mathbf{t}_1 = (\cos\psi, \sin\psi, 0)$.

Step 3: $\hat{\mathbf{N}}_\rho$ lies on $x_1^A y_1^A$ and is perpendicular to $\hat{\mathbf{t}}_1$ as shown in figure 12c). The orientation of coordinate system 0 with respect to A_1 is given by ${}^{A_1}_{0}\mathbf{R} = \mathrm{Rot}(\psi, \hat{\mathbf{k}})$.

Step 4: $\mathcal{S}_1^A$ and $\mathcal{S}_1^B$ are generated by RP dyads that allow permutation. In figure 12b) $\mathcal{S}_1^A$ is generated by the dyad $\{\mathbf{S}_{1,1}, \mathbf{S}_{1,2}\}$ and $\mathcal{S}_1^B$ is generated by $\{\mathbf{S}_{1,6}, \mathbf{S}_{1,5}\}$. To join the end links of both dyads, two revolute joints with axes parallel to the axes of the cylinders and intersecting at E_1 are required. The result is the overconstrained mechanism shown in figure 12b) which is known as the Koenigs joint [5, 24]. At $E_1 = P_1$ its coupler curve has a bifurcation.

Steps 5 and 6: Figure 13 shows the 3-loop mechanism obtained after reflecting the overconstrained linkage obtained in step 4 and adding a coupler bar of length $l = 2$.

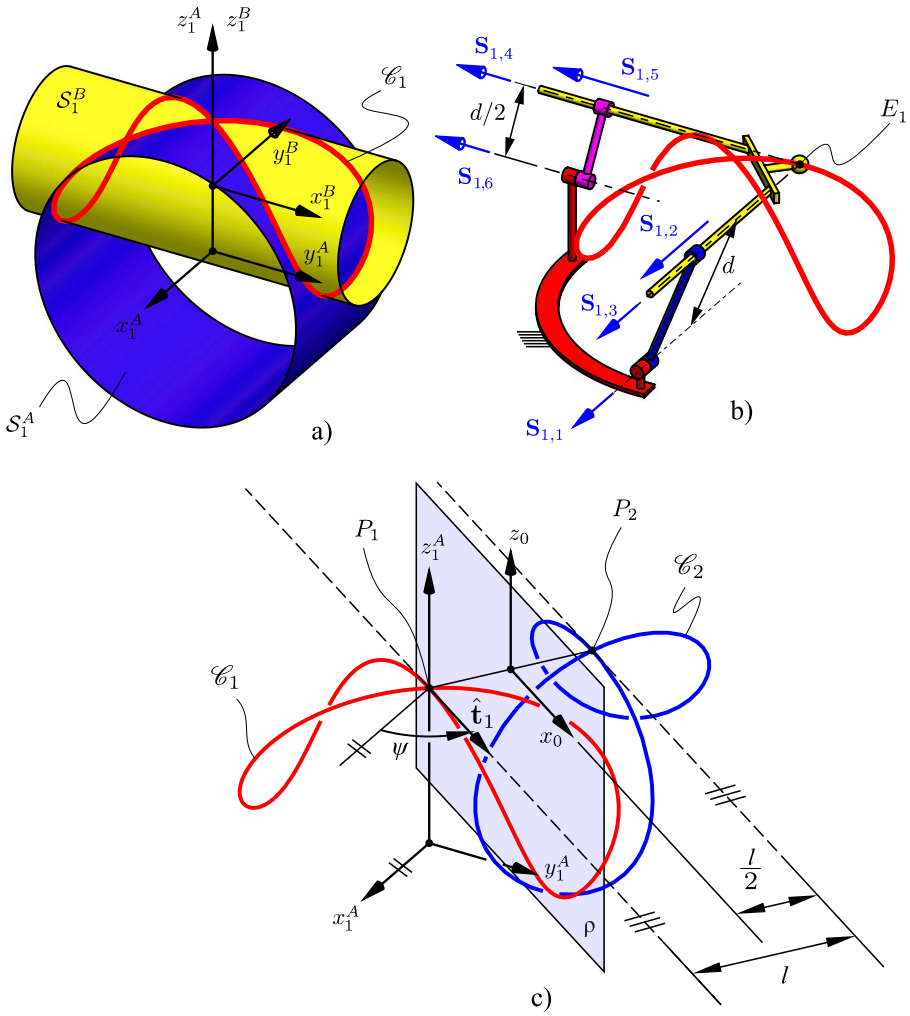

Fig. 12 The intersection of two cylinders that has a projection with an inflection point. a) Surfaces setup. b) The Koenigs joint that generates such intersection. c) reflection of the intersection curve

Analysis of smooth motions through $\mathbf{q}_0$: The screw coordinates at the cusp are

$$\mathbf{S}_{1,1}(\mathbf{q}_0) = \left(\frac{\sqrt{3}}{3}, -\frac{\sqrt{6}}{3}, 0; -\frac{2\sqrt{6}}{3}, -\frac{2\sqrt{3}}{3}, \frac{\sqrt{3}}{3}\right),$$

$$\mathbf{S}_{1,2}(\mathbf{q}_0) = \left(0, 0, 0; \frac{\sqrt{3}}{3}, -\frac{\sqrt{6}}{3}, 0\right),$$

$$\mathbf{S}_{1,3}(\mathbf{q}_0) = \left(\frac{\sqrt{3}}{3}, -\frac{\sqrt{6}}{3}, 0; 0, 0, \frac{\sqrt{3}}{3}\right),$$

$$\mathbf{S}_{1,4}(\mathbf{q}_0) = \left(\frac{\sqrt{6}}{3}, \frac{\sqrt{3}}{3}, 0; 0, 0, \frac{\sqrt{6}}{3}\right),$$

$$\mathbf{S}_{1,5}(\mathbf{q}_0) = \left(0, 0, 0; \frac{\sqrt{6}}{3}, \frac{\sqrt{3}}{3}, 0\right),$$

$$\mathbf{S}_{1,6}(\mathbf{q}_0) = \left(\frac{\sqrt{6}}{3}, \frac{\sqrt{3}}{3}, 0; \frac{\sqrt{3}}{3}, -\frac{\sqrt{6}}{3}, \frac{\sqrt{6}}{3}\right),$$

$$\mathbf{S}_{2,1}(\mathbf{q}_0) = \left(\frac{\sqrt{3}}{3}, \frac{\sqrt{6}}{3}, 0; \frac{2\sqrt{6}}{3}, -\frac{2\sqrt{3}}{3}, -\frac{\sqrt{3}}{3}\right),$$

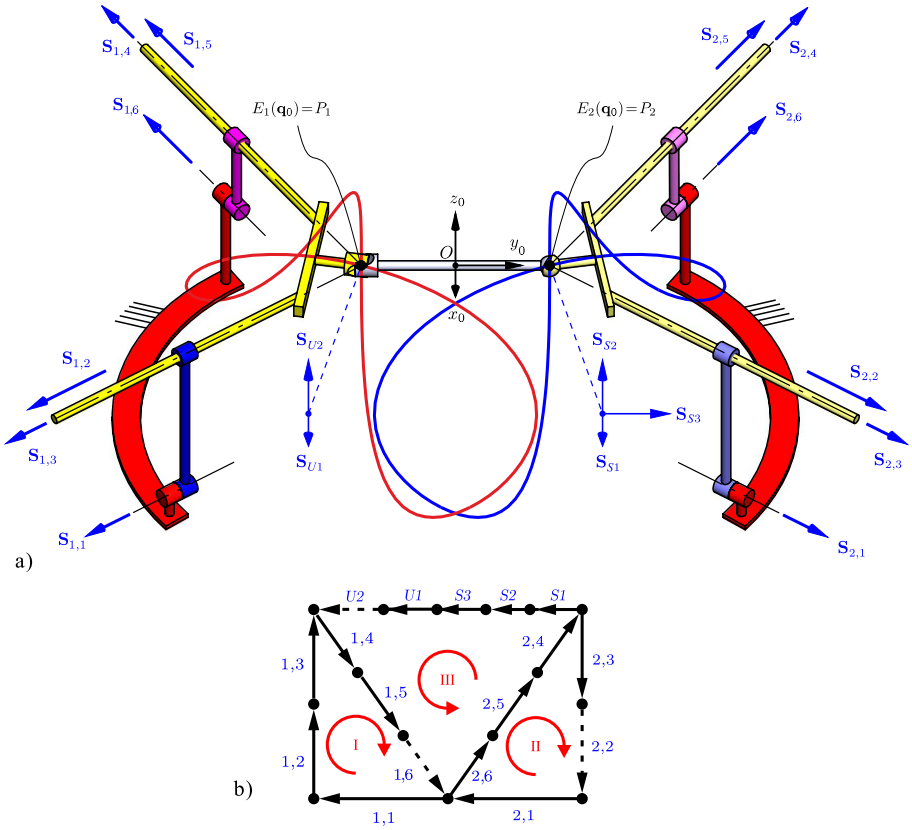

Fig. 13 A double-Koenigs mechanism in a cusp configuration.

$$\mathbf{S}_{2,2}(\mathbf{q}_0) = \left(0,\, 0,\, 0;\, \frac{\sqrt{3}}{3},\, \frac{\sqrt{6}}{3},\, 0\right),$$

$$\mathbf{S}_{2,3}(\mathbf{q}_0) = \left(\frac{\sqrt{3}}{3},\, \frac{\sqrt{6}}{3},\, 0;\, 0,\, 0,\, -\frac{\sqrt{3}}{3}\right),$$

$$\mathbf{S}_{2,4}(\mathbf{q}_0) = \left(\frac{\sqrt{6}}{3},\, -\frac{\sqrt{3}}{3},\, 0;\, 0,\, 0,\, -\frac{\sqrt{6}}{3}\right),$$

$$\mathbf{S}_{2,5}(\mathbf{q}_0) = \left(0,\, 0,\, 0;\, \frac{\sqrt{6}}{3},\, -\frac{\sqrt{3}}{3},\, 0\right),$$

$$\mathbf{S}_{2,6}(\mathbf{q}_0) = \left(\frac{\sqrt{6}}{3},\, -\frac{\sqrt{3}}{3},\, 0;\, -\frac{\sqrt{3}}{3},\, -\frac{\sqrt{6}}{3},\, -\frac{\sqrt{6}}{3}\right),$$

$$\mathbf{S}_{U1}(\mathbf{q}_0) = (1,\, 0,\, 0;\, 0,\, 0,\, 1)\,,$$

$$\mathbf{S}_{U2}(\mathbf{q}_0) = (0,\, 0,\, 1;\, -1,\, 0,\, 0)\,,$$

$$\mathbf{S}_{S1}(\mathbf{q}_0) = (1,\, 0,\, 0;\, 0,\, 0,\, -1)\,,$$

$$\mathbf{S}_{S2}(\mathbf{q}_0) = (0,\, 1,\, 0;\, 0,\, 0,\, 0)\,,$$

$$\mathbf{S}_{S3}(\mathbf{q}_0) = (0,\, 0,\, 1;\, 1,\, 0,\, 0)\,,$$

With these screw coordinates, the kinematic tangent cone is determined as $C^{\mathrm{K}}_{\mathbf{q}_0}V = C^{\mathrm{K}}_{\mathbf{q}_0}V_1 \cup C^{\mathrm{K}}_{\mathbf{q}_0}V_2 \cup C^{\mathrm{K}}_{\mathbf{q}_0}V_3$ where

$$
\begin{aligned}
C^{\mathrm{K}}_{\mathbf{q}_0}V_1 = \big\{\mathbf{x}|\ & x_{11}=x_{12}=x_{13}=x_{14}=x_{15}=x_{16}=0,\\
& x_{U1}=x_{S1}=x_{S2}=0, x_{21}=\tfrac{s}{\sqrt{2}}, x_{22}=10s,\\
& x_{23}=-\tfrac{s}{\sqrt{2}}, x_{24}=-s, x_{25}=-10\sqrt{2}s, x_{26}=s,\\
& x_{U2}=-\sqrt{3}\tfrac{s}{2}, x_{S3}=\sqrt{3}\tfrac{s}{2};\ s\in\mathbb{R}\big\}\\
C^{\mathrm{K}}_{\mathbf{q}_0}V_2 = \big\{\mathbf{x}|\ & x_{11}=\tfrac{s}{\sqrt{2}}, x_{12}=-10s, x_{13}=-\tfrac{s}{\sqrt{2}}, x_{14}=-s,\\
& x_{15}=10\sqrt{2}s, x_{U2}=\tfrac{\sqrt{3}}{2}s, x_{S3}=-\tfrac{\sqrt{3}}{2}s, x_{16}=s,\\
& x_{21}=x_{22}=x_{23}=x_{24}=x_{25}=x_{26}=0,\\
& x_{U1}=x_{S1}=x_{S2}=0;\ s\in\mathbb{R}\big\}\\
C^{\mathrm{K}}_{\mathbf{q}_0}V_3 = \big\{\mathbf{x}|\ & x_{11}=\tfrac{s}{\sqrt{2}}, x_{12}=-10s, x_{13}=-\tfrac{s}{\sqrt{2}}, x_{14}=-s,\\
& x_{15}=10\sqrt{2}s, x_{21}=\tfrac{s}{\sqrt{2}}, x_{22}=10s, x_{23}=-\tfrac{s}{\sqrt{2}},\\
& x_{24}=-s, x_{25}=-10\sqrt{2}s, x_{26}=s, x_{16}=s,\\
& x_{U1}=x_{U2}=x_{S1}=x_{S2}=x_{S3}=0;\ s\in\mathbb{R}\big\}.
\end{aligned}
\tag{5}
$$

Each $C^{\mathrm{K}}_{\mathbf{q}_0}V_i, i=1,2,3$ is a 1-dimensional vector space. These are the tangent spaces to the manifolds V_i intersecting at $\mathbf{q}_0$, shown in figure 14. The motion branches V_4 and V_5 shown in the figure are not smooth manifolds and curves in V_4 and V_5 are not smooth at $\mathbf{q}_0$. Therefore, their tangent aspects are not revealed by the kinematic tangent cone, which consists of tangents to smooth curves.

Discussion on branches: $\mathbf{q}_0 \in V$ is a cusp in the configuration space of the double-Koenigs mechanism when $E_1(\mathbf{q}_0) = P_1$ and $E_2(\mathbf{q}_0) = P_2$. Refer to figure 14. There are two branches, V_1 and V_2, in the configuration space which are cut off at $\mathbf{q}_0$, each related to each of the two solutions explained in Section 4. However, since the self crossing of $\mathscr{C}_i$ is regular in both $\mathcal{S}_i^A$ and $\mathcal{S}_i^B$, $i=1,2$, points E_1 and E_2 are able to move through the other branches of the self-crossings. As a consequence of this, three regular curves, V_1, V_2 and V_3, are intersecting at $\mathbf{q}_0$. These three curves represent smooth motions of E_1 and E_2 through different combination of the branches intersecting at the self-crossings of $\mathscr{C}_1$ and $\mathscr{C}_2$. Figure 14 shows a (regular) configuration of the mechanism in each branch.

6.3 A Kinematotropic Double-Bricard Mechanism

Step 1: Consider the following parametrization:

$$
\begin{aligned}
\sigma(u,v) := \ & d\,((\cos v+1)\cos u - \cos\gamma\sin v\sin u,\\
& \cos\gamma\sin v\cos u + \sin u\cos v + \sin u,\ \sin\gamma\sin v) \in \mathbb{R}^3,
\end{aligned}
$$

so that $\mathcal{S} := \mathrm{im}(\sigma(\mathbb{T}^2))$ is a toroid in which the radius of both the base circle and the secondary circle are d. Thus, it has a conic singularity at the center of the base circle. The tilting angle between the planes containing the secondary

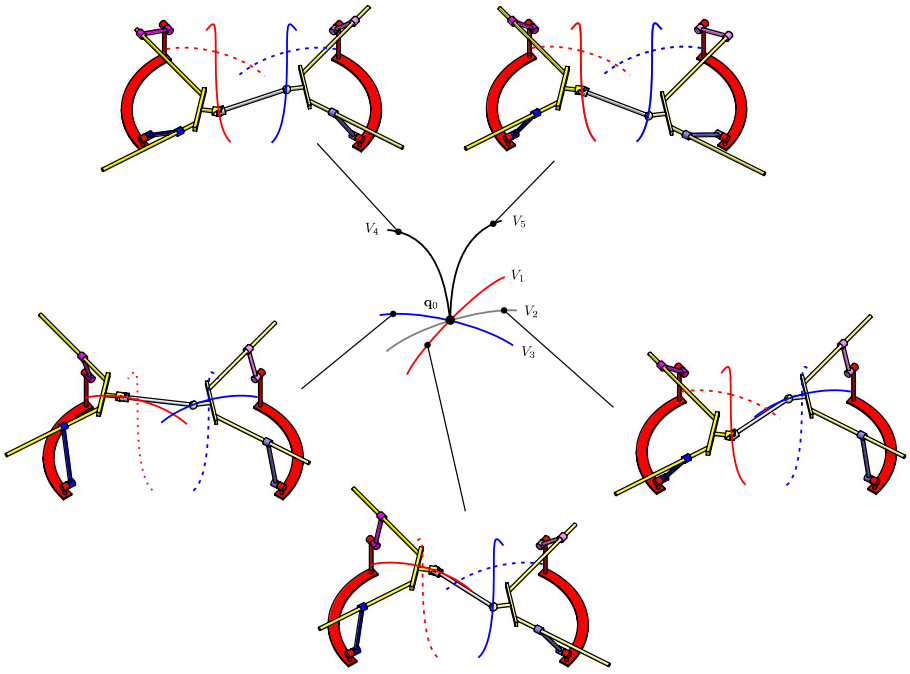

Fig. 14 Different branches of the configuration space intersecting at $\mathbf{q}_0$.

circle and the base circle is γ and the axis of the toroid is the $z-$axis. Consider the toroids $\mathcal{S}_1^A := \text{im}(\sigma_1^A(\mathbb{T}^2))$, where ${}^{A_1}\sigma_1^A(u,v) := \sigma(u,v)$ with $d = 3$ and $\gamma = \pi/4$, and $\mathcal{S}_1^B := \text{im}(\sigma_1^B(\mathbb{T}^2))$, where ${}^{B_1}\sigma_1^B(u,v) := \sigma(u,v)$ with $d = 4$ and $\gamma = \pi/6$. The origins of frames A_1 and B_1 coincide and their relative orientation is given by ${}^{A_1}_{B_1}\mathbf{R} := \text{Rot}(\pi/4, \hat{\mathbf{j}})$ as shown in figure 15a). $\mathscr{C}_1$ is an 8-shaped curve that is symmetric with respect to the $x_1^A z_1^A$ plane. Moreover, one of the two wings is obtained by rotating the other wing π radians about the $y_1^A = y_1^B$ axis. Therefore, its projection onto the $y_1^A z_1^A$ plane[3] has an inflection point at the projection of the self-crossing. We set P_1 at the self crossing, as shown in figure 15c).

Step 2: Since P_1 is a singularity in $\mathcal{S}_1^A$ and $\mathcal{S}_1^B$ there is no local information available. $\hat{\mathbf{t}}_1$ and $\hat{\mathbf{t}}_2$ can, however, be easily obtained by finding the intersection of two right cones with half angles $\pi/2 - \alpha_{1,1-1,2} = \pi/4$ and $\pi/2 - \alpha_{1,6-1,5} = \pi/3$ and the same axes of revolution as $\mathcal{S}_1^A$ and $\mathcal{S}_1^B$, respectively. Since a toroid with a singularity at the origin is tangent to a cone whose singularity coincides with that of the toroid and whose half angle is $\pi/2$ minus the tilting angle between the base and secondary circle, the intersection of two toroids of this

[3] A parametrization of $\mathscr{C}$ is not difficult to be obtained due to the symmetries of the surfaces. With such parametrization it can be proved that $\mathscr{C}$ has zero curvature at P_1 and, hence, the Frenet apparatus is not defined. Due to such anomaly, a plane onto which $\mathscr{C}$ can be projected to obtain an inflection point is not unique. In this case the projection onto any plane containing $\hat{\mathbf{t}}_1$ has an inflection point.

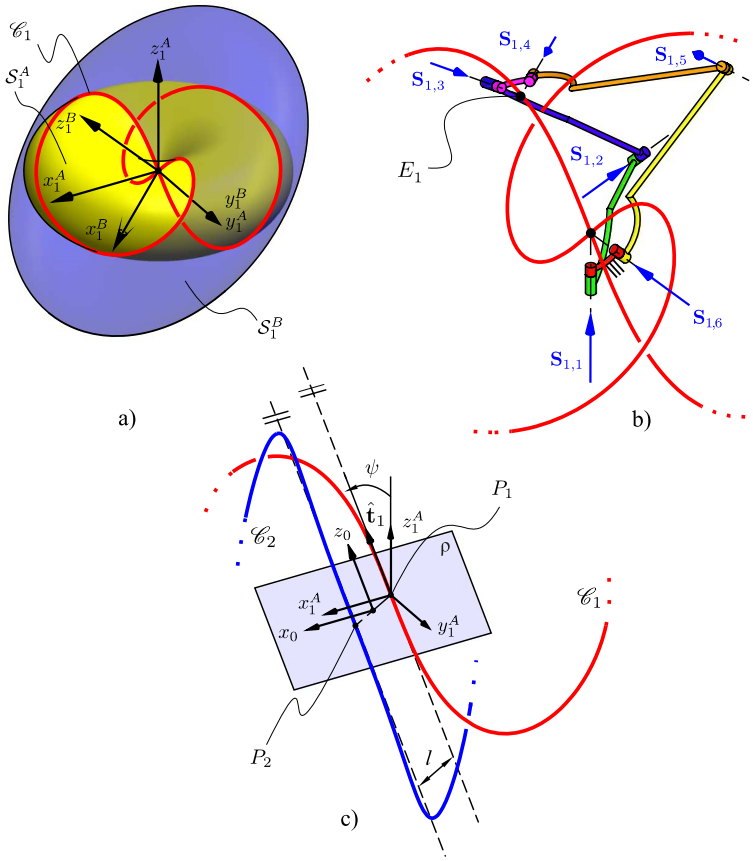

Fig. 15 The intersection of two toroids that has a projection with an inflection point. a) Surfaces setup. b) The Bricard plane-symmetric 6R mechanism that generates such intersection. c) reflection of the intersection curve.

kind is tangent to the lines obtained by intersecting the cones that are tangent to the toroids at the singularity. The two tangents are ${}^{A_1}\hat{\mathbf{t}}_1 = (0, -\sqrt{2}/2, \sqrt{2}/2)$ and $\hat{\mathbf{t}}_2 = (0, \sqrt{2}/2, \sqrt{2}/2)$. We choose $\hat{\mathbf{t}}_1$, to perform the reflection.

Step 3: $\hat{\mathbf{N}}_\rho$ lies in the $y_1^A z_1^A$ plane and is perpendicular to $\hat{\mathbf{t}}_1$ as shown in figure 15c). The orientation of coordinate system 0 with respect to A_1 is given by ${}^{A_1}_{0}\mathbf{R} = \mathrm{Rot}(\psi, \hat{\mathbf{i}})$, where $\psi = \pi/4$ is obtained from $\hat{\mathbf{t}}_1$.

Step 4: Figure 15b) shows the mechanism that generates such intersection. $\mathcal{S}_1^A$ is generated by the point E_1 of the dyad $\{\mathbf{S}_{1,1}, \mathbf{S}_{1,2}\}$, while $\mathcal{S}_1^B$ is generated by the point E_1 of the dyad $\{\mathbf{S}_{1,1}, \mathbf{S}_{1,2}\}$. $\mathbf{S}_{1,1}$ and $\mathbf{S}_{1,6}$ are along z_1^A and z_1^B, so they can generate the base circles (see [13]). Observe that since the radii of the secondary and base circles are the same, the distance between E_1 and $\mathbf{S}_{1,2}$ (E_1 and $\mathbf{S}_{1,5}$) is the same as the link length $a_{11,12} = 3$ ($a_{16,15} = 4$), where $a_{1i,1j}$ is the normal distance between the axes of $\mathbf{S}_{1,i}$ and $\mathbf{S}_{1,j}$. This symmetry allows the assembling of a plane-symmetric Bricard mechanism [3–

5] in figure 16 where the spherical joint at E_1 is reduced to a pair of revolute joints $\mathbf{S}_{1,3}$ and $\mathbf{S}_{1,4}$. The plane of symmetry is that containing the permanently intersecting axes $\mathbf{S}_{1,2}$ and $\mathbf{S}_{1,5}$. The twist angles $\alpha_{1,1-1,2} = \pi/4$ and $\alpha_{1,6-1,5} = \pi/6$ are the value of γ for $\mathcal{S}_1^A$ and $\mathcal{S}_1^B$, respectively. $a_{1,1-1,2} = a_{1,2-1,3} = 3$ and $a_{1,6-1,5} = a_{1,5-1,4} = 4$ are the radii of both the base and the secondary circles of $\mathcal{S}_1^A$ and $\mathcal{S}_1^B$, respectively. The twist angle $\alpha_{1,1-1,6} = \pi/4$ is the angle between the axes of the toroids (angle between z_1^A and z_1^B), and, due to symmetry, $\alpha_{1,3-1,4} = \alpha_{1,1-1,6}$. The Denavit-Hartenberg (DH) parameter [11] for axial displacement is zero for all joints, therefore, the toroids are symmetric with respect to the plane containing their base circles. Observe that when E_1 coincides with the singularities of the toroids, the revolute joints with axes $\mathbf{S}_{1,1}$, $\mathbf{S}_{1,2}$, $\mathbf{S}_{1,3}$ and $\mathbf{S}_{1,4}$ constitute a spherical 4-bar mechanism. Once this mechanism starts moving the plane symmetry is broken and revolute joints with axes $\mathbf{S}_{1,2}$ and $\mathbf{S}_{1,5}$ become idle. The mechanism enters in a spherical 4-bar operation mode with E_1 remaining coincident with the singularities of the toroids during this motion. A special line- and plane-symmetric Bricard mechanism presenting the same reconfiguration to a spherical 4-bar linkage was presented in [6]. The line-symmetric Bricard linkages obtained as the intersection of two toroids was first analyzed in [29].

It is important to mention, that since $P_1 \in \text{sing}(\mathcal{S}_1^A) \cap \text{sing}(\mathcal{S}_1^B)$, E_1 is unable to move from one branch to another at P_1, see [29] for an in-depth analysis of this singularity. Therefore, unlike in the Koenigs joint, in this Bricard mechanism the two branches of the configuration space, V, related to the two branches of $\mathscr{C}_1$ intersecting at P_1 are not intersecting when $E_1 = P_1$ and, thus, $\exists\, \mathbf{q}_1, \mathbf{q}_2 \in V$ such that $\mathbf{q}_1 \neq \mathbf{q}_2$ and $E_1(\mathbf{q}_1) = E_1(\mathbf{q}_2) = P_1$.

Steps 5 and 6: Figure 16 shows the 3-loop mechanism obtained after reflecting the overconstrained linkage obtained in step 4 and adding the coupler bar.

Analysis of smooth motions through $\mathbf{q}_0$: The screw coordinates at the cusp are

$$
\begin{aligned}
\mathbf{S}_{1,1}(\mathbf{q}_0) &= \left(0,\, \frac{\sqrt{2}}{2},\, \frac{\sqrt{2}}{2};\, 5\sqrt{2},\, 0,\, 0\right),\\
\mathbf{S}_{1,2}(\mathbf{q}_0) &= (0,\, 1,\, 0;\, 0,\, 0,\, -30)\,,\\
\mathbf{S}_{1,3}(\mathbf{q}_0) &= \left(0,\, \frac{\sqrt{2}}{2},\, -\frac{\sqrt{2}}{2};\, -5\sqrt{2},\, 0,\, 0\right),\\
\mathbf{S}_{1,4}(\mathbf{q}_0) &= \left(\frac{\sqrt{2}}{2},\, \frac{1}{2},\, -\frac{1}{2};\, -5,\, 0,\, -5\sqrt{2}\right),\\
\mathbf{S}_{1,5}(\mathbf{q}_0) &= \left(\frac{\sqrt{6}}{3},\, \frac{\sqrt{3}}{3},\, 0;\, 0,\, 0,\, -40 - \frac{10\sqrt{6}}{3}\right),
\end{aligned}
$$

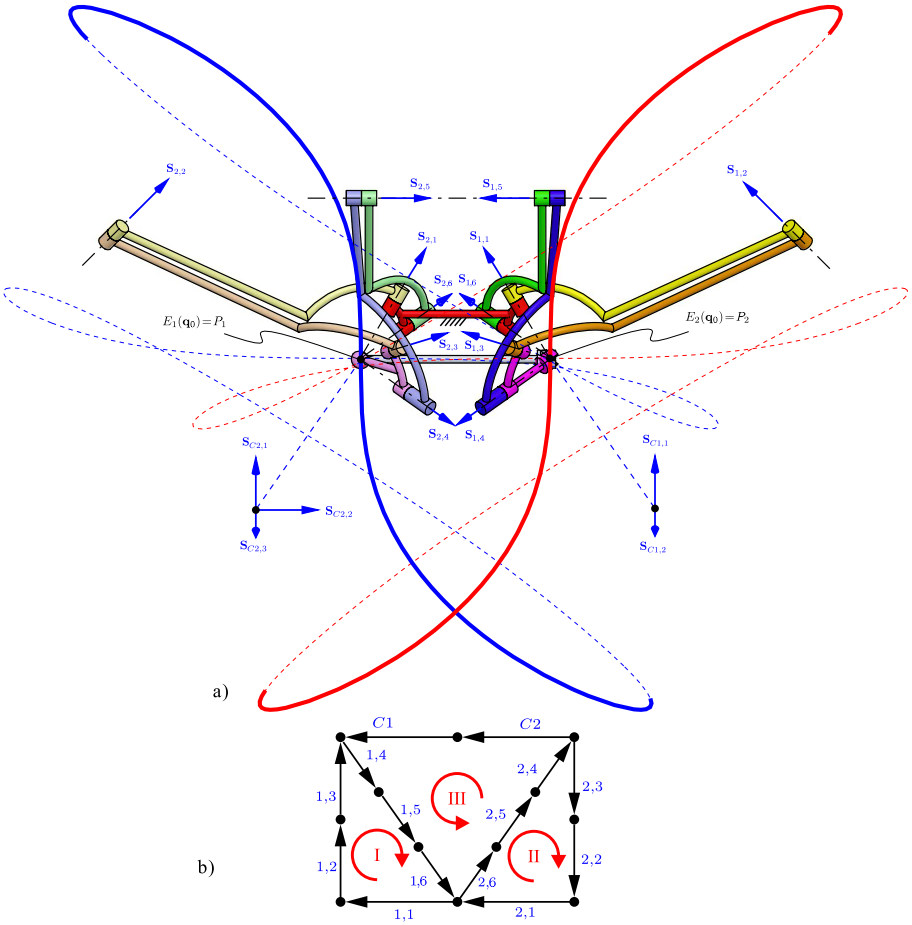

Fig. 16 A double-Bricard mechanism in a cusp configuration.

$$\mathbf{S}_{U1}(\mathbf{q}_0) = (1,\, 0,\, 0;\, 0,\, 0,\, -10)\,,$$
$$\mathbf{S}_{U2}(\mathbf{q}_0) = (0,\, 0,\, 1;\, 10,\, 0,\, 0)\,,$$
$$\mathbf{S}_{1,6}(\mathbf{q}_0) = \left(\frac{\sqrt{2}}{2},\, \frac{1}{2},\, \frac{1}{2};\, 5,\, 0,\, -5\sqrt{2}\right),$$
$$\mathbf{S}_{2,1}(\mathbf{q}_0) = \left(0,\, -\frac{\sqrt{2}}{2},\, \frac{\sqrt{2}}{2};\, -5\sqrt{2},\, 0,\, 0\right),$$
$$\mathbf{S}_{2,2}(\mathbf{q}_0) = (0,\, -1,\, 0;\, 0,\, 0,\, 30)\,,$$
$$\mathbf{S}_{2,3}(\mathbf{q}_0) = \left(0,\, -\frac{\sqrt{2}}{2},\, -\frac{\sqrt{2}}{2};\, 5\sqrt{2},\, 0,\, 0\right),$$
$$\mathbf{S}_{2,4}(\mathbf{q}_0) = \left(\frac{\sqrt{2}}{2},\, -\frac{1}{2},\, -\frac{1}{2};\, 5,\, 0,\, 5\sqrt{2}\right),$$
$$\mathbf{S}_{2,5}(\mathbf{q}_0) = \left(\frac{\sqrt{6}}{3},\, -\frac{\sqrt{3}}{3},\, 0;\, 0,\, 0,\, 40 + \frac{10\sqrt{6}}{3}\right),$$

$$\begin{aligned}
\mathbf{S}_{2,6}(\mathbf{q}_0) &= \left(\frac{1}{2}\sqrt{2},\, -\frac{1}{2},\, \frac{1}{2};\, -5,\, 0,\, 5\sqrt{2}\right), \\
\mathbf{S}_{S1}(\mathbf{q}_0) &= (1,\, 0,\, 0;\, 0,\, 0,\, 10)\,, \\
\mathbf{S}_{S2}(\mathbf{q}_0) &= (0,\, 1,\, 0;\, 0,\, 0,\, 0)\,, \\
\mathbf{S}_{S3}(\mathbf{q}_0) &= (0,\, 0,\, 1;\, -10,\, 0,\, 0)\,.
\end{aligned} \tag{6}$$

With these screw coordinates, the kinematic tangent cone is determined as

$$\begin{aligned}
C^{\mathrm{K}}_{\mathbf{q}_0} V = \{\mathbf{x}|\ & x_{11} = \tfrac{s}{\sqrt{2}}, x_{12} = 0, x_{13} = -\tfrac{s}{\sqrt{2}}, x_{14} = s, x_{15} = 0, x_{16} = -s, \\
& x_{21} = -\tfrac{t}{\sqrt{2}}, x_{22} = 0, x_{23} = \tfrac{t}{\sqrt{2}}, x_{24} = -t, x_{25} = 0, x_{26} = t, \\
& x_{U1} = 0, x_{U2} = s, x_{S1} = 0, x_{S2} = 0, x_{S3} = -t;\ s, t \in \mathbb{R}\}.
\end{aligned} \tag{7}$$

This is the tangent space to the manifold V_3 shown in figure 16. The branches V_1 and V_2 shown in the figure are not smooth manifolds and curves in V_1 and V_2 are not smooth at $\mathbf{q}_0$.

Discussion on branches: Since, in the cusp configuration presented in figure 16 $E_1 = P_1$ and $E_2 = P_2$ both Bricard loops are able to enter the spherical 4-bar operation mode explained above. During this motion, E_1 and E_2 remain coincident with P_1 and P_2, respectively. The coupler bar restricting the position of E_1 and E_2 remains static and there is no restriction between the motion of loops I and II. Hence, from $\mathbf{q}_0$ the mechanism can enter a 2-DOF branch of motion with partitioned mobility [37]. Figure 17 shows a 3-dimensional section of the c-space near the cusp.

7 Conclusions

This paper presented for the first time a method for the design of spatial 1-DOF mechanisms that exhibit a cusp in their configuration space. The method was obtained by extending the idea presented by Connelly and Servatius in their double-Watt linkage which is a planar cusp mechanism. Such a linkage takes advantage of the inflection point of the curve drawn by the middle point of the coupler link of each of the two 4-bar Watt linkages. In this paper, this idea was extended to the spatial case in order to design spatial 1-DOF cusp mechanisms. It was found that a simple way of dealing with curves traced by spatial mechanisms is the use of intersection of surfaces generated [26, 28, 29, 44] by kinematic dyads. Using this method, three examples were presented. It was shown that the c-spaces of two of these examples not only present the cusp singularity, but also have other motion branches intersecting at such a singularity, leading to very complex c-spaces that are difficult to analyze. For every example, a local approximation of smooth motions was computed by means of the kinematic tangent cone. While this provides a sufficient local description at non-cuspidal c-space singularities (bifurcations), it is shown that this is not true at cusps. The presented analysis thus shows the need for additional research into the singularity analysis. The development of such analysis methods has not been a topic of research simply because the phenomenon is widely

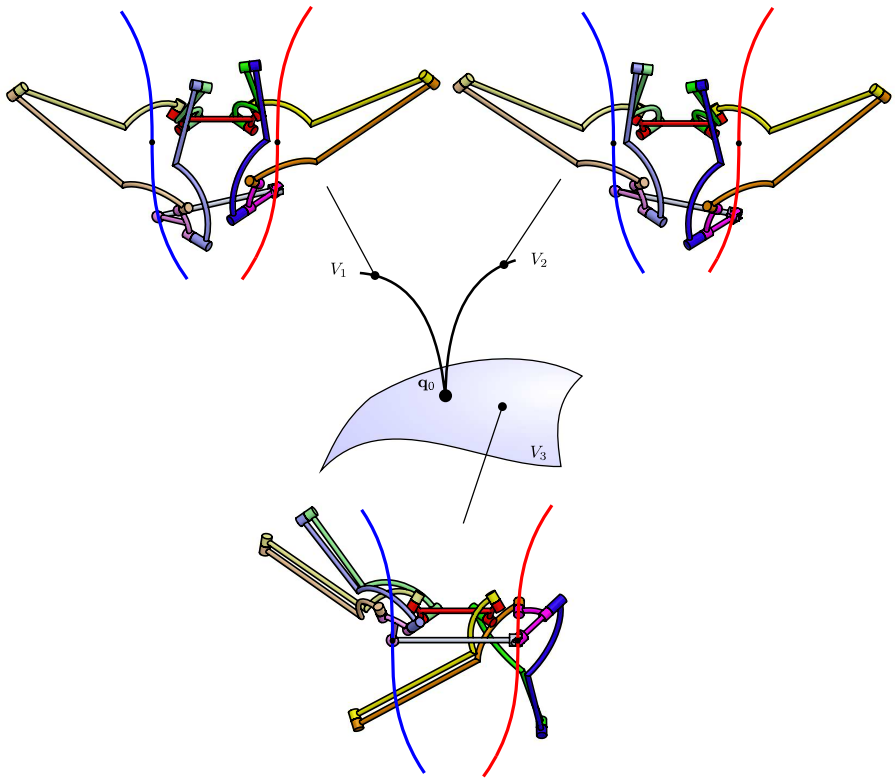

Fig. 17 Different branches of the configuration space intersecting at $\mathbf{q}_0$.

unknown, given that only Connelly and Servatius have presented an example. The presented synthesis method and examples are aimed to provide spatial 1-DOF test cases. A straight-forward approach to the cusp singularity analysis is the local approximation of the c-space using Taylor series expansion of the constraints. This can be formalized [35] in the framework of screw theory.

The existence of mechanisms with higher-order cusps in their configuration space was further discussed in this paper by providing a planar example. Such a mechanism (a double-Evans linkage) was designed by noting that a 4-bar Evans mechanism can draw a curve that approximates a straight line up to the fifth order at an inflection point.

To the knowledge of the authors the examples presented in this paper are the first cusp mechanisms presented after Connelly's double-Watt linkage and the mechanism recently presented by the authors of this paper in [30]. All the examples presented in this paper can be used in the study of cusp singularities and as challenges for proposed methods of local analysis of mechanisms.

Acknowledgements P.C. López-Custodio thanks The Mexican National Council for Science and Technology (CONACyT), the Ministry of Public Education (SEP) and the Advanced Kinematics and Reconfigurable Robotics Lab at King's College for the support

awarded to pursue doctoral studies. A. Müller acknowledges that work has been supported by the "LCM K2 Center for Symbiotic Mechatronics" within the framework of the Austrian COMET-K2 program. P.C. López-Custodio and J.S. Dai acknowledge the support of the Engineering and Physical Sciences Research Council (EPSRC) projects with reference numbers EP/P025447/1 and EP/P026087/1.

References

1. Aimedee F, Gogu G, Dai J, Bouzgarrou C, Bouton N (2016) Systematization of morphing in reconfigurable mechanisms. Mechanism and Machine Theory 96, Part 2:215 – 224, DOI 10.1016/j.mechmachtheory.2015.07.009
2. Angeles J (2012) Spatial Kinematic Chains: Analysis Synthesis Optimization. Springer-Verlag Berlin Heidelberg, Heidelberg, Germany
3. Baker JE (1980) An analysis of the Bricard linkages. Mechanisms and Machine Theory 15:267–286, DOI 10.1016/0094-114X(80)90021-X
4. Bricard R (1897) Mémoire sur la thèorie de l'octaèdre articulè. Journal of Pure and Applied Mathematics 3:113–150
5. Bricard R (1927) Leçons de cinématique. Gauthier-Villars, Paris, France
6. Chen Y, Chai WH (2011) Bifurcation of a special line and plane symmetric bricard linkage. Mechanism and Machine Theory 46(4):515 – 533, DOI 10.1016/j.mechmachtheory.2010.11.015
7. Chiang C (2000) Kinematics of Spherical Mechanisms. Krieger Publishing Company, Malabar, FL, USA
8. Connelly R, Servatius H (1994) Higher-order rigidity—what is the proper definition? Discrete & Computational Geometry 11(2):193–200, DOI 10.1007/BF02574003
9. Crane C, Duffy J (1998) Kinematic analysis of robot manipulators. Cambridge: Cambridge University Press, Cambridge, UK
10. Dai JS, Gogu G (2016) Special issue on reconfigurable mechanisms: Morphing, metamorphosis and reconfiguration through constraint variations and reconfigurable joints. Mechanism and Machine Theory 96, Part 2:213 – 214, DOI 10.1016/j.mechmachtheory.2015.11.006
11. Denavit J, Hartenberg RS (1955) A kinematic notation for lower-pair mechanisms based on matrices. ASME Journal of Applied Mechanics 23:215–221
12. Ferguson ES (1962) Kinematics of Mechanisms from the Time of Watt. Smithsonian Institution, Washington D.C., USA
13. Fichter EF, Hunt KH (1975) The fecund torus, its bitangent-circles and derived linkages. Mechanism and Machine Theory 10(2-3):167–176, DOI 10.1016/0094-114X(75)90017-8
14. Gibson C, Hunt K (1990) Geometry of screw systems - 1. Mechanism and Machine Theory 25(1):1 – 10, DOI 10.1016/0094-114X(90)90103-Q
15. Gibson C, Hunt K (1990) Geometry of screw systems - 2: classification of screw systems. Mechanism and Machine Theory 25(1):11 – 27, DOI 10.1016/0094-114X(90)90104-R

16. Hervé JM (1978) Analyse structurelle des mécanismes par groupe des déplacements. Mechanism and Machine Theory 13(4):437–450, DOI 10.1016/0094-114X(78)90017-4
17. Hortobágyi Z (2000) Numerical analysis of inextensional, kinematically indeterminate assemblies. Periodica Polytechnica Civil Engineering 44(1):43 – 55, DOI N/A
18. Hunt KH (1978) Kinematic Geometry of Mechanisms. Oxford University Press, New York, USA
19. Jenkins EM, Crossley FRE, Hunt KH (1969) Gross motion attributes of certain spatial mechanisms. Journal of Engineering for Industry 91(1):83–90, DOI 10.1115/1.3591557
20. Kempe A (1877) How to Draw a Straight Line: A Lecture on Linkages. Macmillan and Company, London, UK
21. Kreyszig E (1959) Differential Geometry. University of Toronto Press, Toronto, Canada
22. Kühnel W (2002) Differential Geometry: Curves - Surfaces - Manifolds. Europe and Central Asia Environmentally and Socially Sustain, American Mathematical Society, Providence, RI, USA
23. Kuznetsov E (1999) Singular configurations of structural systems. International Journal of Solids and Structures 36(6):885 – 897, DOI 10.1016/S0020-7683(97)00333-8
24. Lee CC, Hervé JM (2012) A discontinuously movable constant velocity shaft coupling of Koenigs joint type. In: JS Dai MZ, Kong X (eds) Advances in Reconfigurable Mechanisms and Robots I, pp 35–43, DOI 10.1007/978-1-4471-4141-9_4
25. Litvin F, Yi Z, Castelli VP, Innocenti C (1986) Singularities, configurations, and displacement functions for manipulators. The International Journal of Robotics Research 5(2):52–65, DOI 10.1177/027836498600500206
26. López-Custodio P, Rico J, Cervantes-Sánchez J, Pérez-Soto G (2016) Reconfigurable mechanisms from the intersection of surfaces. ASME Journal of Mechanisms and Robotics 8(2):021,029–1—021,029–19
27. López-Custodio P, Rico J, Cervantes-Sánchez J (2017) Local analysis of helicoid-helicoid intersections in reconfigurable linkages. ASME Journal of Mechanisms and Robotics Accepted paper
28. López-Custodio PC, Dai JS, Rico JM (2018) Branch reconfiguration of Bricard linkages based on toroids intersections: Line-symmetric case. ASME Journal of Mechanisms and Robotics 10(3):031,002–031,002–12, DOI doi: 10.1115/1.4038981
29. López-Custodio PC, Dai JS, Rico JM (2018) Branch reconfiguration of bricard linkages based on toroids intersections: Plane-symmetric case. ASME Journal of Mechanisms and Robotics 10(3):12 pages, DOI 10.1115/1.4039002
30. López-Custodio PC, Müller A, Dai JS (2018) The double-Koenigs mechanism – a spatial linkage with cusp singularities and multiple branches in the configuration space –. In: Proceedings of the 4th IEEE/IFToM In-

ternational Conference on Reconfigurable Mechanisms and Robots, Delft, The Netherlands
31. Lu DM, Hwang WM (1996) Spherical four-bar linkages with symmetrical coupler-curves. Mechanism and Machine Theory 31(1):1 – 10, DOI 10.1016/0094-114X(95)00049-5
32. Müller A (2002) Local analysis of singular configurations of open and closed loop manipulators. Multibody System Dynamics 8(3):297–326, DOI 10.1023/A:1020969529920
33. Müller A (2016) Local kinematic analysis of closed-loop linkages –mobility, singularities, and shakiness. ASME Journal of Mechanisms and Robotics 8(4):11 pages, DOI 10.1115/1.4032778
34. Müller A (2018) Higher-order analysis of kinematic singularities of lower pair linkages and serial manipulators. ASME Journal of Mechanisms and Robotics 10(1):(13 pages), DOI 10.1115/1.4038528
35. Müller A (2018) A screw approach to the approximation of the local geometry of the configuration space and of the set of configurations of certain rank of lower pair linkages. In: International Design Engineering Technical Conferences and Computers and Information in Engineering Conference, Quebec, Canada
36. Rico JM, Ravani B (2002) Group theory can explain the mobility of paradoxical linkages. In: Lenarčič J, Thomas F (eds) Advances in Robot Kinematics, Springer Netherlands, Dordrecht, pp 245–254, DOI 10.1007/978-94-017-0657-5_26
37. Rico JM, Ravani B (2003) On mobility analysis of linkages using group theory. Transactions of the ASME: Journal of Mechanical Design 125(1):70–80, DOI 10.1115/1.1541628
38. Sabitov IK (1994) On the relations between infinitesimal bendings of different orders. Journal of Mathematical Sciences 72(4):3237–3241, DOI 10.1007/BF01249526
39. Shirazi K (2005) Symmetrical coupler curve and singular point classification in planar and spherical swinging-block linkages. ASME Journal of Mechanisms and Robotics 128(2):436 – 443, DOI 10.1115/1.2167651
40. Shirazi K (2009) A study of the Jacobian matrix of serial manipulators. ASME Journal of Mechanisms, Transmissions and Automation in Design 107(2):230 – 237, DOI 10.1115/1.3258714
41. Sugimoto K, Duffy J, Hunt K (1982) Special configurations of spatial mechanisms and robot arms. Mechanism and Machine Theory 17(2):119 – 132, DOI 10.1016/0094-114X(82)90042-8
42. Tarnai T, Szabó J (2000) Finite mechanisms have no higher-order rigidity. Acta Technica Acad Sci- Hung 106(3):119 – 125, DOI 10.1016/S0045-7949(99)00090-5
43. Tarnai T, Szabó J (2000) On the exact equation of inextensional, kinematically indeterminate assemblies. Computers & Structures 75(2):145 – 155, DOI 10.1016/S0045-7949(99)00090-5
44. Torfason LE, Crossley FRE (1971) Use of the intersection of surfaces as a method for design of spatial mechanisms. In: Proceedings of the 3rd

World Congress for the Theory of Machines and Mechanisms, Kupari, Yugoslavia, vol **B**, pp 247–258, paper B-20
45. Ye X, Maekawa T (1999) Differential geometry of intersection curves of two surfaces. Computer Aided Geometric Design 16(8):767 – 788, DOI 10.1016/S0167-8396(99)00018-7
46. Zlatanov D, Bonev I, Gosselin C (2002) Constraint singularities as configuration space singularities. In: Lenarčič J, Thomas F (eds) Advances in Robot Kinematics, Springer Netherlands, pp 183–192, DOI 10.1007/978-94-017-0657-5_20